
VLM-RobustBench: A Comprehensive Benchmark for Robustness of Vision-Language Models

Rohit Saxena¹ Alessandro Suglia¹ Pasquale Minervini^{1,2}

Abstract

Vision-language models (VLMs) achieve strong performance on standard, high-quality datasets, but we still do not fully understand how they perform under real-world image distortions. We present **VLM-RobustBench**, a benchmark spanning 49 augmentation types across noise, blur, weather, digital, and geometric perturbations, evaluated under graded severities (low/mid/high) and binary transforms, yielding 133 corrupted settings. We evaluate VLMs from four families (Qwen, InternVL, Molmo, Gemma) on two complementary benchmarks: MMBench (visually grounded) and MMMU-Pro (reasoning-oriented). Our results reveal that visual severity is a weak predictor of difficulty: low-severity spatial perturbations often degrade performance more than visually severe photometric corruptions. In particular, low-severity `glass_blur` reduces MMBench accuracy by about 8 pp on average across models, while the largest drops arise from resampling and geometric distortions (e.g., `upsample`, `elastic_transform`), reaching up to 34 pp. Overall, our findings suggest current VLMs are *semantically strong but spatially fragile*, motivating the definition of novel robustness evaluation protocols and training regimes that emphasize resampling and geometric invariances.

1. Introduction

The rapid evolution of Vision-Language Models (VLMs) has marked a transition from text-only specialists to multimodal generalist models that are capable of complex reasoning across a broad range of tasks. Recent VLMs (Bai et al., 2025; Clark et al., 2026; Wang et al., 2025a; Team et al., 2025) demonstrated remarkable proficiency on several benchmarks, exhibiting capabilities ranging from zero-shot generalisation to fine-grained image-text understand-

ing (Liu et al., 2024). These advancements catalysed the integration of VLMs into safety-critical pipelines, including autonomous driving perception stacks (Zhou et al., 2024), medical diagnostic support systems (Sellergren et al., 2025), and automated document processing workflows (Wang et al., 2025b).

However, strong performance on curated benchmarks does not guarantee reliability under the distribution shifts encountered in deployment (Yu et al., 2024). Real-world visual inputs are rarely pristine: low-light sensor noise, adverse weather (rain, fog, snow), compression artefacts, and motion or defocus blur are common (Hendrycks & Dietterich, 2019). In addition, viewpoint changes induce geometric variations, such as scaling, rotation, and perspective distortion, that may be absent or simplified in training data (Barbu et al., 2019b; Zhou et al., 2022). For safety-critical use, we therefore need robustness evaluations that stress these everyday corruptions rather than measuring accuracy on a fixed dataset that includes only a few visual perturbations.

While the computer vision community has established rigorous benchmarks for robustness to common corruptions—most notably ImageNet-C (Hendrycks & Dietterich, 2019), the robustness landscape for modern VLMs remains less systematically characterised, especially across tasks and realistic corruption families (Usama et al., 2025; Ye et al., 2024). A central challenge is understanding whether language-side reasoning can compensate when visual perception is degraded, or whether certain perturbations induce sharp perceptual bottlenecks that dominate end performance (Liu et al., 2025; Fan et al., 2025; Zhou et al., 2025).

Moreover, corruption benchmarks often implicitly assume *severity monotonicity*: as visual distortion increases, inputs should become increasingly harder (Hendrycks & Dietterich, 2019). It remains unclear whether this assumption holds for VLMs, where perception and language reasoning are tightly coupled through cross-modal representations (Zhou et al., 2025). This motivates a dedicated benchmark that probes the interplay between visual corruptions and multimodal reasoning across a broad spectrum of perturbation types and severity levels.

¹University of Edinburgh, UK ²Miniml.AI. Correspondence to: Rohit Saxena <rohit.saxena@ed.ac.uk>.

In this work, we present **VLM-RobustBench**, a large-scale analysis of VLM robustness under visual corruption. We systematically evaluate 11 models spanning four major VLM families (Qwen, InternVL, Molmo, and Gemma) across 133 distinct augmentation configurations (42 corruptions at three severities plus 7 binary transforms) on two diverse datasets: MMBench (Liu et al., 2024) (more visually grounded) and MMMU-Pro (Yue et al., 2025) (more reasoning-oriented). Our results challenge prevailing assumptions and reveal that current VLMs are *semantically strong but spatially fragile*. We highlight three key contributions:

1. **The Spatial Fragility Finding:** VLMs are disproportionately sensitive to spatial and resampling artefacts. A resampling operation (`upsample`) or mild geometric distortion causes catastrophic failure (up to 34pp drop), whereas severe photometric degradations (e.g., noise, compression) are often handled robustly.
2. **Severity Mismatch:** We observe a decoupling of severity level and model difficulty (Figure 1). On MMBench, low-severity perturbations degrade performance more than high-severity perturbations of other types, complicating safety assurance (e.g., `glass_blur` and `solarize` at low severity result in an 8pp and 5.6pp drop, respectively).
3. **Family-Specific Vulnerabilities:** Robustness is not a function of parameter count. Distinct model families exhibit unique vulnerability “fingerprints,” suggesting that architectural choices play a decisive role in determining failure modes.

2. Related Work

Vision–language model evaluation benchmarks. The rapid progress of large vision–language models (LVLMs) has driven a parallel effort on standardised evaluation. Widely used benchmarks measure complementary aspects of multimodal capability, including broad multi-skill perception and reasoning (Liu et al., 2024), discipline-spanning expert knowledge and reasoning (MMMU and its variant MMMU-Pro) (Yue et al., 2024; 2025), and structured decompositions of perception versus cognition (Fu et al., 2025). Beyond aggregate scores, recent work highlights that some VLMs can answer via language priors with limited visual grounding (Tong et al., 2024), motivating “vision-centric” evaluations such as NaturalBench (Li et al., 2024) that reduce “blind” shortcuts. Our work builds on this evaluation ecosystem but focuses on reliability under visual degradations, using MMBench (more visually grounded) and MMMU-Pro (more reasoning-oriented) to ensure a robust assessment. Additionally, we use *visual gain* to quantify directly reliance on visual information versus language priors.

Robustness to natural corruptions in vision. Robustness to common, naturally occurring corruptions has a long history in computer vision, formalised by benchmarks such as ImageNet-C/ImageNet-P (Hendrycks & Dietterich, 2019), which apply parameterised families of noise, blur, weather, digital, and geometric perturbations with calibrated severities. Related benchmarks extend distribution shift beyond corruptions, including style/rendition shifts (ImageNet-R) (Hendrycks et al., 2021) and view-point/background changes (ObjectNet) (Barbu et al., 2019a). VLM-RobustBench follows the corruption-benchmark philosophy but adapts it to LVLM settings, expanding the augmentation taxonomy and explicitly separating graded severities from binary transforms to reflect real deployment conditions (e.g., resampling artefacts, watermarks, borders).

Natural-corruption robustness in VLMs and VQA. Compared to vision-only models, the robustness of LVLMs under visual corruption is less mature. Recent studies evaluate VLMs under subsets of ImageNet-C-like corruptions and introduce corrupted VQA settings, highlighting sensitivity patterns that differ across tasks (Usama et al., 2025). Our benchmark differs in (i) breadth of corruptions (including resampling and geometry-focused stressors and VLM-specific artefacts), (ii) explicit severity analysis (low/mid/high) alongside binary transforms, and (iii) evaluation on both visually grounded and reasoning-oriented multimodal benchmarks, enabling analysis of when models fall back to language priors versus visual grounding.

Adversarial robustness of vision–language models. A distinct line of work studies worst-case, adversarial perturbations for vision–language pretraining models and LVLMs, including transferable and black-box attacks (Zhao et al., 2023; Qi et al., 2024; Shayegani et al., 2024), as well as defences that robustify the vision encoder or the multimodal alignment. Canonical demonstrations show that adversarial images can circumvent safeguards and induce incorrect or unsafe generations in multimodal models (Carlini et al., 2023). On the defence side, adversarially fine-tuning CLIP-style encoders (e.g., Robust CLIP) can improve robustness for downstream LVLMs that rely on frozen vision backbones (Mao et al., 2023). While adversarial robustness is crucial for security, our focus is complementary: we target naturally occurring corruptions and operational artifacts that arise in the absence of an adaptive attacker, and we show that these “benign” perturbations can dominate tail risk.

Spatial robustness and resolution effects. Our main finding, high sensitivity to spatial/resampling corruptions, connects to robustness properties of patch-based encoders. Prior work analyses robustness of Vision Transformers under corruptions and distribution shift, motivating architectural and training choices for improved invariances (Bhojanapalli



Figure 1. **The Severity Paradox.** On MMBench (mean over 9 models), high-severity brightness reduction (center) causes only a 1.6pp accuracy drop, while low-severity glass blur (right) causes an 8.1pp drop. Severity level does not always predict model difficulty.

et al., 2021; Paul & Chen, 2022). In the LVLM context, preprocessing choices (e.g., resizing strategy, tokenization granularity) can materially affect performance (McKinzie et al., 2024). VLM-RobustBench provides a systematic corruption suite to quantify these effects at scale and to guide robustness-oriented training curricula that emphasize geometric and resampling invariances.

3. Method

3.1. Problem Formulation

Let \mathcal{M} denote a vision-language model that takes an image $I \in \mathcal{I}$ from the space of images $\mathcal{I} = \mathbb{R}^{H \times W \times 3}$ and a text query Q as input, producing a textual response $\mathcal{M}(I, Q)$. We evaluate multiple-choice accuracy using an answer extractor $g(\cdot)$ that maps the response to a discrete option, yielding $\hat{y} = g(\mathcal{M}(I, Q))$.

We define a set of image augmentations $\mathcal{A} = \{A_1, \dots, A_K\}$. Each severity-based augmentation A_k is a stochastic transformation parameterized by severity $s \in \mathcal{S}$ that maps an image $I \in \mathcal{I}$ to one of its augmented versions $\hat{I} \in \mathcal{I}$, with $\hat{I} \sim A_k(I, s)$. For reproducibility, we fix per-sample random seeds, yielding deterministic outputs for each (image, severity) pair. Binary augmentations are not parameterised by s and apply directly as $A_k(I)$.

Given a dataset $\mathcal{D} = \{(I_i, Q_i, y_i)\}_{i=1}^N$ with ground-truth answers y_i , we define clean accuracy as:

$$\text{Acc}_{\text{clean}} = \frac{1}{N} \sum_{i=1}^N \mathbf{1}[g(\mathcal{M}(I_i, Q_i)) = y_i],$$

and accuracy under augmentation A_k at severity s as:

$$\text{Acc}_{A_k, s} = \frac{1}{N} \sum_{i=1}^N \mathbf{1}[g(\mathcal{M}(A_k(I_i, s), Q_i)) = y_i]. \quad (1)$$

The robustness drop $\Delta_{A_k, s} = \text{Acc}_{\text{clean}} - \text{Acc}_{A_k, s}$ quantifies the performance degradation in percentage points. We addi-

tionally evaluate a no-image baseline Acc_{\emptyset} where images are removed.

Visual Gain. To quantify reliance on visual information versus language priors, we define *Visual Gain* (VG) as

$$\text{VG} = \text{Acc}_{\text{clean}} - \text{Acc}_{\emptyset}. \quad (2)$$

A larger VG indicates stronger dependence on visual input, whereas a low VG suggests greater solvability from language priors alone.

Relative Corruption Error. To normalize corruption impact by a model’s visual reliance, we define

$$\text{RCE}_{A_k, s} = \frac{\Delta_{A_k, s}}{\text{VG}} \times 100\%. \quad (3)$$

All model–dataset pairs in our experiments have $\text{VG} > 7$, so division is well-defined. $\text{RCE}=100\%$ means the corruption removes all visual benefit; $\text{RCE}>100\%$ means performance becomes worse than the no-image baseline.

3.2. Augmentation Taxonomy

We construct a suite of 49 image augmentations motivated by real-world degradations. The suite comprises 42 severity-based corruptions grouped into nine categories and 7 binary transforms (Table 1). Each severity-based corruption is evaluated at three levels $s \in \{\text{low, mid, high}\}$, whereas binary transforms are applied once (no severity parameter).

For corruptions overlapping ImageNet-C (Hendrycks & Dettlerich, 2019), we reuse the same corruption types but calibrate severity levels independently for VLM evaluation. For VLM-specific corruptions, we define monotonic, visually ordered severity schedules (full parameter schedules in Section C.5). Low severity corresponds to mild perturbations, while high severity corresponds to strongly degraded inputs. This yields 126 severity-based configurations (42×3 levels) plus 7 binary transforms, resulting in 133 augmentation configurations per model–dataset pair.

Category	N	Augmentations
Blur	5	Gaussian, motion, defocus, glass, zoom
Noise	4	Gaussian, shot, speckle, salt-pepper
Weather	5	Fog, frost, snow, rain, spatter
Digital	2	JPEG compression, pixelation
Geometric	5	Rotate, shear, affine, perspective_transform, elastic
Occlusion	3	Center, random, grid mask
Color/Tone	10	Brightness [±] , contrast [±] , saturation [±] , gamma [±] , hue shift, color jitter
Resolution	5	Downsample, upsample, sharpen, posterize, solarize
VLM-specific	3	Text overlay, watermark, border
Binary	7	Grayscale, invert, equalize, autocontrast, channel swap, flip (h/v)

Table 1. Augmentation taxonomy. We group 42 severity-based corruptions into nine categories and evaluate each at low/mid/high; 7 binary transforms are applied once. Superscript [±] denotes separate increase/decrease variants.

Family	Model	Type
Qwen3-VL	Qwen3-VL-4B	Instruct
	Qwen3-VL-8B	Instruct
	Qwen3-VL-30B-A3B	MoE, 3B active
	Qwen3-VL-4B-Think	Thinking
	Qwen3-VL-8B-Think	Thinking
InternVL3.5	InternVL3.5-4B	Instruct
	InternVL3.5-8B	Instruct
	InternVL3.5-14B	Instruct
Molmo2	Molmo2-4B	Instruct
	Molmo2-8B	Instruct
Gemma 3	Gemma-3-12B-it	Instruct

Table 2. Family of VLMs evaluated. Main comparisons use the 9 instruct checkpoints in standard prompting; Qwen Think models are reported separately as a test-time compute ablation.

4. Experimental Setup

4.1. Models

We evaluate **11 VLMs** spanning four model families of open-weights models: Qwen3-VL (Bai et al., 2025), InternVL3.5 (Wang et al., 2025a), Molmo2 (Clark et al., 2026), and Gemma3 (Team et al., 2025) (Table 2). Our primary robustness comparisons focus on *9 instruction-following VLMs* evaluated under a consistent direct-answer prompting protocol. We additionally include **2 Qwen3-VL Think** models (4B and 8B) as a *test-time compute ablation*. To isolate the role of reasoning at inference time, we compare chain-of-thought prompting against the Think variants ¹.

¹These results are reported in Section A.4 and are not included in the main aggregate robustness comparisons.

4.2. Datasets

We evaluate on two challenging multimodal benchmarks (with seed 42 for reproducibility):

MMMU-Pro A professional-level multimodal understanding benchmark covering subjects from STEM to humanities. We use the standard 10-option multiple choice variant, evaluating on a stratified 20% sample (532 samples) across 30 subject categories.

MMBench A comprehensive benchmark for multimodal perception and reasoning. We evaluate on the English development split using stratified 20% sampling (869 samples) to ensure category balance across all question types.

4.3. Evaluation Protocol

For each model-dataset pair, we evaluate on clean images, a no-image baseline (image removed), and all corrupted settings: 126 severity-based configurations (42 corruptions \times 3 severity levels) plus 7 binary transforms, totaling *133 + 2 (baseline) evaluations* per pair. Corruptions are applied to images only; text prompts and answer formats are held fixed across conditions. We use stratified 20% subsampling above to keep the full corruption sweep tractable (135 settings per model-dataset pair) while preserving category balance.

Unless stated otherwise, we report results in direct mode (standard prompting) and aggregate over the 9 instruction-following checkpoints. Chain-of-thought (CoT) and thinking results are reported separately in Section A.4.

Metrics. We report clean accuracy $\text{Acc}_{\text{clean}}$ as defined in Section 3.1. Since mean accuracy aggregates across augmentation types and severities, it can mask severity-specific and tail failures; we therefore focus on drop-based metrics that highlight failure modes. For each configuration (A_k, s) , we define the accuracy drop (in percentage points) as $\Delta_{A_k, s} = \text{Acc}_{\text{clean}} - \text{Acc}_{A_k, s}$ (binary transforms omit s).

We additionally report: (i) *Worst-Case Drop* $\max_{k, s} \Delta_{A_k, s}$, the maximum drop over all 133 configurations (126 severity-based + 7 binary); (ii) *Severe-Failure Rate*, the fraction of the same 133 configurations for which performance drops by more than a relative threshold, $\Delta_{A_k, s} > 0.1 \text{Acc}_{\text{clean}}$. (iii) *Worst@Low* $\max_k \Delta_{A_k, \text{low}}$, the maximum drop over 42 severity-based corruptions at low severity (binary excluded); and (iv) *Benign@Low*, the fraction of these 42 low-severity corruptions with $\Delta \leq 1$. Additional implementation details are in Section C.

5. Results

5.1. Tiered Robustness Overview

Table 3 provides a tiered snapshot of robustness in direct mode. We report $\text{Acc}_{\text{clean}}$ (*Baseline*) alongside drop-based

MMBench (Direct)							
Model	Baseline \uparrow	Worst-Case \downarrow	Severe-Fail \downarrow	Worst@Low \downarrow	Benign@Low \uparrow	VG \uparrow	mRCE \downarrow
Qwen3-VL-4B	88.4	26.3	3.8	7.0	88.1	48.2	3.9
Qwen3-VL-8B	90.2	30.2	5.3	8.3	73.8	48.2	5.2
Qwen3-VL-30B	90.7	29.4	3.8	6.1	88.1	47.7	3.5
InternVL3.5-4B	86.3	30.5	9.8	10.8	64.3	44.9	7.7
InternVL3.5-8B	89.1	31.7	8.3	9.6	71.4	50.8	6.5
InternVL3.5-14B	86.6	29.4	9.0	9.5	88.1	44.5	6.0
Molmo2-4B	88.5	33.1	4.5	7.4	78.6	43.6	5.5
Molmo2-8B	88.4	33.9	4.5	6.3	90.5	48.4	4.4
Gemma-3-12B	85.3	32.1	8.3	10.7	69.0	44.1	6.4

MMMUPro (Direct)							
Model	Baseline \uparrow	Worst-Case \downarrow	Severe-Fail \downarrow	Worst@Low \downarrow	Benign@Low \uparrow	VG \uparrow	mRCE \downarrow
Qwen3-VL-4B	31.5	7.4	3.8	2.8	95.2	7.1	-6.8
Qwen3-VL-8B	35.2	9.0	7.5	5.2	85.7	11.4	4.7
Qwen3-VL-30B	40.7	14.5	12.8	7.4	59.5	17.0	12.1
InternVL3.5-4B	37.3	11.1	14.3	5.6	76.2	12.3	11.6
InternVL3.5-8B	41.0	12.3	16.5	5.6	45.2	14.2	16.5
InternVL3.5-14B	42.0	9.6	9.0	5.9	85.7	15.1	5.2
Molmo2-4B	31.8	5.6	3.8	4.3	92.9	12.0	4.9
Molmo2-8B	31.2	5.6	5.3	4.0	90.5	7.4	1.0
Gemma-3-12B	33.0	9.9	27.1	9.0	28.6	10.8	24.2

Table 3. Main robustness summary (9 direct-mode models). Worst-Case and Severe-Fail are computed over all 133 configurations (126 severity-based + 7 binary). Worst@Low and Benign@Low are computed over the 42 low-severity configurations only (binary excluded). mRCE is the mean Relative Corruption Error over all $|C| = 133$ configurations. VG and RCE are defined in Section 3.1.

tail-risk summaries that capture how models fail across the full corruptions: *Worst-Case Drop*, *Severe-Failure Rate*, *Worst@Low*, and *Benign@Low*. These metrics are deployment-relevant because robustness risk is often dominated by a small number of failure-inducing transformations (e.g., resampling in a preprocessing pipeline), even when most corruptions are harmless. We additionally report *VG* (visual reliance) and *mRCE* (mean relative corruption error) to normalize corruption impact by how much each model benefits from vision (Section 3.1).

Two patterns stand out. First, *large failures are sparse but consequential*: on MMBench, many low-severity corruptions are benign (typically $\Delta \leq 1$ for about 65–90% of the 42 low-severity settings, depending on the model), yet a small subset produces sharp accuracy drops. This is reflected by the *Severe-Failure Rate*, which measures how often a model experiences a drop larger than 0.1 $\text{Acc}_{\text{clean}}$ across the 133 configurations. For example, InternVL3.5-4B attains a severe-failure rate of 9.8% on MMBench, meaning 13 out of 133 corrupted settings exceed this threshold.

Second, *visually mild perturbations can still be high-risk*. *Worst@Low* shows that even at low severity, some corruptions cause substantial degradation (up to 10.8 pp on MMBench). In contrast, MMMUPro exhibits a wider spread in *Benign@Low* (roughly 30–95% of the 42 low-severity settings), consistent with varying degrees of visual reliance

across models and tasks.

Preempting the “destroyed image” intuition. Although high-severity corruptions can visibly degrade inputs, our main takeaway is that perceived visual severity is a weak predictor of difficulty: subtle spatial perturbations (e.g., low-severity `glass_blur` and resampling artifacts) can be as harmful as, or more harmful than, strong photometric distortions (e.g., JPEG compression).

5.2. Binary Augmentations: Trivial Transforms, Large Failures

Beyond the 126 severity-based configurations, our 133-config benchmark includes 7 binary (on/off) augmentations. Table 4 reveals that two trivial transformations—vertical flip and color inversion—are *catastrophic* on MMBench despite requiring no learned parameters.

Key insight. Vertical flip is more harmful than 39 of 42 high-severity corruptions on MMBench, exceeded only by `upsample`, `elastic_transform`, and `zoom_blur`—suggesting VLMs encode strong orientation priors. Color inversion causes catastrophic drops on MMBench (10.1pp) but only mild harm on MMMUPro (1.4pp), indicating perception tasks depend on absolute color relationships while reasoning does not.

Perception vs. Reasoning via Visual Gain. We analyze Vi-

Augmentation	MMBench		MMMU-Pro	
	Drop	Tier	Drop	Tier
Autocontrast	0.0	Benign	-0.2	Benign
Grayscale	3.2	Moderate	0.4	Benign
Channel Swap	3.2	Moderate	0.0	Benign
Equalize	3.5	Moderate	0.3	Benign
Horizontal Flip	6.9	Moderate	3.6	Moderate
Invert	10.1	Catastrophic	1.4	Mild
Vertical Flip	10.3	Catastrophic	4.2	Moderate

Table 4. Binary augmentation drops (pp) averaged over 9 direct-mode models. Vertical flip and color inversion cause catastrophic failures on MMBench ($\Delta > 10$ pp); vertical flip exceeds the mean drop of 39 out of 42 high-severity corruptions.

sual Gain ($VG = Acc_{clean} - Acc_{\emptyset}$) as a proxy for reliance on visual input versus language priors. VG is computed per model and then averaged across direct-mode models. MMBench has substantially larger VG (46.7 points) than MMMU-Pro (11.9 points), indicating that MMBench decisions depend more strongly on visual grounding, whereas MMMU-Pro permits greater fallback to language priors. This aligns with MMBench exhibiting larger worst-case drops and higher severe-failure rates (Table 3).

5.3. Which Corruptions Drive Risk?

Figure 2 shows the most harmful corruptions at each severity, averaged over all direct-mode models. Per-model breakdowns are in Section A.8. Two consistent patterns emerge. First, *severity is an unreliable proxy for difficulty*: at low severity, `glass_blur` (8.1 drop on MMBench, 5.5 on MMMU-Pro) is among the top failures, exceeding most high-severity corruptions. Second, *catastrophic risk concentrates in a small set of resampling and geometric corruptions*: `upsample` and `elastic_transform` dominate mid/high severities on MMBench, while `zoom_blur` becomes more prominent on MMMU-Pro.

Glass Blur Anomaly. Low-severity `glass_blur` outperforms many high-severity photometric corruptions (e.g., JPEG compression), providing a concrete example of the severity-difficulty mismatch. Interestingly, `glass_blur` exhibits non-monotonic behaviour, with low severity sometimes inducing larger drops than higher severities (Section A.9), further illustrating the decoupling of visual and model difficulty.

5.4. Quantifying Severity Mismatch

Severity mismatch can be quantified by checking whether performance degrades monotonically with increasing visual severity. For each model and severity-based corruption A_k , we compute: (i) A *monotonicity violation* indicator, set to 1 if $\Delta_{A_k,low} > \Delta_{A_k,mid}$ or $\Delta_{A_k,mid} > \Delta_{A_k,high}$ (strict inequality; ties do not count as violations), and 0 otherwise.

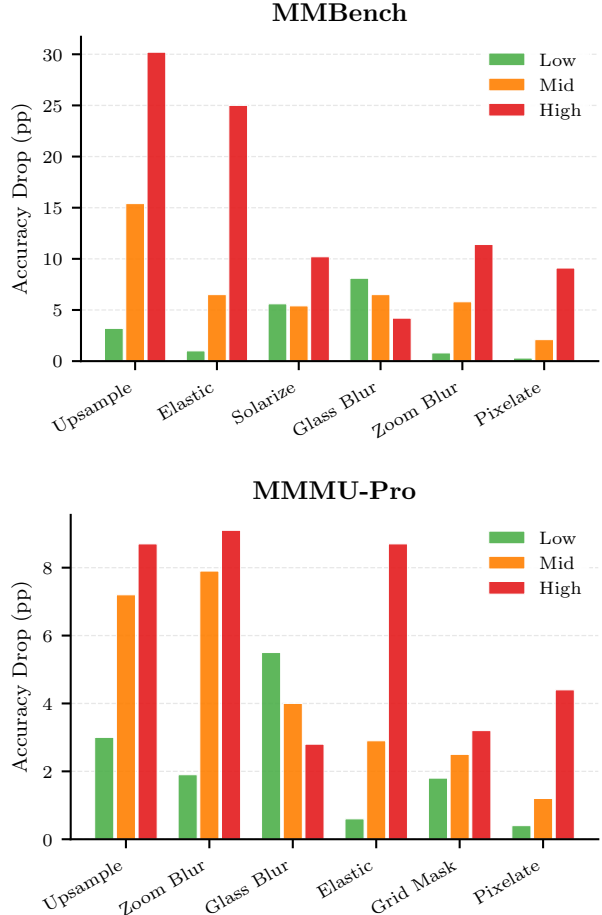


Figure 2. Top corruptions by severity (mean drop, 9 models). Resampling corruptions (`upsample`, `elastic_transform`) dominate at mid/high severity, while `glass_blur` shows an inverted pattern (Low > Mid > High) on both datasets.

(ii) The Spearman rank correlation (ρ) between severity level {low, mid, high} and the robustness drop. All corruptions are deterministic given fixed parameters and per-sample seeds; we do not average over multiple stochastic draws, so observed violations reflect true model behavior rather than sampling variance.

We report these metrics in Section B.1. Overall, we observe substantial violation rates and weak-to-moderate correlations, indicating that visually ordered severity is an unreliable proxy for model difficulty, particularly on reasoning-oriented MMMU-Pro.

5.5. Catastrophic vs. Mild Distribution

Let $\Delta_{A_k,s} = Acc_{clean} - Acc_{A_k,s}$ denote the accuracy drop (percentage points). We define tiers: *benign* ($\Delta \leq 1$), *mild* ($1 < \Delta \leq 3$), *moderate* ($3 < \Delta \leq 10$), *catastrophic* ($\Delta > 10$), and *positive* ($\Delta < 0$, i.e., corruption improves

accuracy). Table 18 reports tier distributions by severity level (direct mode, 9 models \times 42 severity-based augmentations per level, plus 9×7 binary). A key finding: *binary augmentations on MMBench have the same catastrophic count (9) as mid-severity*, despite being trivial transforms—further evidence that spatial manipulations (flips) and color inversions are disproportionately harmful.

5.6. RCE Analysis: Severity Trends and Adversarial Regimes

RCE (defined in Section 3.1) normalizes corruption impact by visual reliance, enabling comparison across models with different VG. We report the *mean RCE over all 133 configurations*: $mRCE = \frac{1}{|C|} \sum_{c \in C} RCE_c$, and additionally report severity-sliced means (Low/Mid/High over 42 configs each) and Binary (7 configs) in Table 20.

RCE by Severity. Table 20 reports mean RCE across models. On MMBench, RCE escalates from 1.6% (low) to 9.7% (high) to 11.5% (binary). MMMU-Pro shows higher RCE despite lower absolute drops because its smaller Visual Gain (11.9 vs. 46.7 points) amplifies relative impact. Notably, two configurations on MMMU-Pro exceed 100% RCE (upsample:high and elastic.transform:high for Qwen3-VL-4B), indicating truly adversarial corruptions.

Model-Specific RCE. Table 3 includes per-model RCE and Visual Gain. On MMBench, InternVL3.5-4B has the highest RCE (7.7%), losing nearly 8% of its visual contribution on average, while Qwen3-VL-30B is most resilient (3.5%). On MMMU-Pro, Gemma-3-12B suffers 24.2% RCE—corruptions destroy nearly a quarter of its visual benefit. Most strikingly, *Qwen3-VL-4B achieves negative RCE (-6.8%) on MMMU-Pro*, meaning corruptions *improve* performance relative to clean images, confirming its minimal visual reliance on reasoning tasks.

Worst-Case RCE by Augmentation. Table 5 lists the top corruptions by RCE. On MMBench, upsample:high destroys 65.6% of visual contribution—over half the benefit of having an image. On MMMU-Pro, zoom.blur:high reaches 77.6% RCE, and two configurations exceed 100% (adversarial). Binary transforms (e.g., flip_v) achieve 22% RCE on MMBench despite being trivial operations, confirming their outsized impact relative to visual reliance.

5.7. Mean Corruption Error (mCE)

Following ImageNet-C (Hendrycks & Dietterich, 2019), we compute *mean Corruption Error (mCE)* to compare model robustness against a reference baseline. For each corruption type c , we define:

$$CE_c = \frac{\sum_s E_{c,s}^{\text{model}}}{\sum_s E_{c,s}^{\text{ref}}} \quad (4)$$

Dataset	Augmentation	Sev.	RCE (%)
MMBench	upsample	high	65.6
	elastic.transform	high	53.8
	upsample	mid	33.5
	zoom.blur	high	24.7
	solarize	high	22.6
	flip_v	binary	22.1
MMMU-Pro	zoom.blur	high	77.6
	elastic.transform	high	73.3
	upsample	high	72.9
	zoom.blur	mid	63.9
	upsample	mid	58.1
	glass.blur	low	44.6

Table 5. Top corruptions by Relative Corruption Error and corresponding severity levels.

Model	MMBench mCE	MMMU-Pro mCE
Qwen3-VL-30B	62.9	89.0
Qwen3-VL-8B	70.8	95.0
Qwen3-VL-4B	77.5	98.9
Molmo2-8B	78.2	100.0 (ref)
Molmo2-4B	79.2	100.0
InternVL3.5-8B	81.2	89.1
InternVL3.5-14B	92.0	85.0
InternVL3.5-4B	98.3	93.1
Gemma-3-12B	100.0 (ref)	101.1

Table 6. Mean Corruption Error (mCE) following ImageNet-C methodology. Lower is better; 100% matches the reference model.

where $E = 1 - \text{Acc}$ is the error rate. For the 42 severity-based corruptions, errors are summed over $s \in \{\text{low, mid, high}\}$; for the 7 binary corruptions, a single error term is used. The reference model is the one with the lowest baseline accuracy (analogous to AlexNet): *Gemma-3-12B* for MMBench (85.3%) and *Molmo2-8B* for MMMU-Pro (31.2%). Mean CE aggregates across all 49 corruption types: $mCE = \frac{1}{49} \sum_c CE_c$.

Table 6 reveals that *Qwen3-VL-30B is the most robust model on MMBench* with only 62.9% of the reference error rate, while *InternVL3.5-14B leads on MMMU-Pro at 85.0%*. Notably, mCE rankings differ from RCE rankings because mCE compares absolute error rates across models, while RCE measures each model’s degradation relative to its own visual contribution. This complementary view shows that models with high baseline accuracy (Qwen family) tend to have lower mCE, while models with high visual gain but moderate baselines (InternVL3.5) show better RCE but higher mCE. In summary, we use tail-risk metrics (worst-case drop, severe-failure rate) for deployment risk assessment, mCE for cross-model robustness ranking, and RCE to factor out language-prior reliance.

5.8. Qualitative Analysis of Failure Modes

Figure 3 and Figure 14 in Section D visualize all 49 augmentations applied to a representative image. A clear pattern emerges: the most damaging corruptions are those that alter *spatial structure* rather than appearance. Low-severity spatial transformations such as `glass_blur`, `upsample`, and `elastic_transform` often induce larger accuracy drops than visually severe photometric distortions such as noise, compression, or color shifts. This suggests that VLMs rely heavily on spatial consistency and alignment, and are disproportionately sensitive to resampling artifacts that disrupt object boundaries or relative geometry. In contrast, degradations that preserve global structure—even when visually strong—are comparatively well tolerated.

Why spatial fragility? We hypothesize this vulnerability stems from the patch-based architecture of Vision Transformers underlying most VLMs. When local patch structures are rearranged or distorted by effects like glass blur or elastic transformations, the pretrained patch embeddings may become misaligned with the learned representations. Resampling operations (`upsample`, `downsample`) introduce interpolation artifacts that similarly disrupt the expected patch statistics. In contrast, photometric changes (brightness, noise, compression) preserve local spatial relationships, allowing the vision encoder to maintain coherent feature extraction. This pattern is consistent across the top rankings in Figure 2, where resampling and geometry-changing corruptions repeatedly appear among the most harmful, including at low severity.

Flip-rate evidence. To isolate behavioral failures beyond mean drops, we measure answer-flip rates (correct on clean \rightarrow incorrect under corruption). Spatial/resampling corruptions induce substantially higher flip rates than photometric corruptions on MMBench (see Appendix A.12).

Systemic vs. Unique Failures. Catastrophic pairs are largely shared across models. On MMBench, the top catastrophic pairs are consistently `upsample:high`, `elastic_transform:high`, and `upsample:mid`. MMMU-Pro catastrophic pairs are rare overall; when they occur, `zoom_blur` (at mid and high severity) and `elastic_transform:high` are the most common culprits. Most catastrophic failures are systemic rather than architecture-specific (see Section A.1 for per-model breakdowns).

Resampling Dominates Tail Risk. Across datasets, catastrophic pairs and worst-case augmentations are dominated by resampling or geometry-changing operations (e.g., `upsample`, `elastic_transform`, `zoom_blur`), consistent with Appendix A.1. Interpolation artifacts appear to be a primary driver of failure. We quantify their contribution to catastrophic cases ($\Delta > 10$) in Appendix B.2.

Family-Specific Vulnerabilities

Severe-failure shares vary by model family and do not track parameter count. On MMBench, severe-failure rates range from 3.8% (Qwen3-VL-4B/30B) to 9.8% (InternVL3.5-4B). Family-specific gaps are pronounced: `shot_noise:high` drops Gemma by 12.9 points vs Qwen by 5.12, `pixelate:high` drops InternVL by 12.97 vs Qwen by 6.06, and `downsample:high` drops InternVL by 9.73 vs Qwen by 4.92. A compact family-by-augmentation matrix is provided in Appendix A.7; detailed family-level breakdowns for representative corruptions appear in Appendix A.9.

6. Conclusion

We presented VLM-RobustBench, a comprehensive benchmark exposing that current VLMs are *semantically strong but spatially fragile*. Our evaluation of 11 open-weights state-of-the-art LVLMs, with sizes ranging from 4B to 30B parameters, across 49 augmentation types reveals several counter-intuitive findings: (1) visual severity does not predict model difficulty—low-severity `glass_blur` (8–11pp drop) outperforms most high-severity corruptions; (2) trivial binary transforms can be catastrophic—vertical flipping (10.3pp) and color inversion (10.1pp) exceed most high-severity corruptions on MMBench; and (3) resampling artifacts (`upsample`, `elastic_transform`) cause catastrophic failures up to 34pp across all models, and (4) our visual reliance evaluation highlights how certain benchmarks are more visually grounded (i.e., MMBench) while others heavily rely on language priors (i.e., MMMU-Pro).

Recommendations for VLM Development.

- Geometric Data Augmentation:** Training pipelines must move beyond color jitter and mixup to include heavy resampling, elastic deformations, flips, and blur augmentations during pretraining.
- Robustness-Aware Evaluation:** Benchmarks should report performance on spatial corruption splits (e.g., “clean vs. flipped vs. resampled”) to penalize models brittle to simple geometric changes.
- Visual reliance:** Model providers should provide results for truly visually grounded language inputs to showcase their models’ ability to perform visually grounded inferences.
- Family-Specific Curricula:** Different architectures exhibit distinct vulnerability fingerprints (e.g., InternVL3.5 is flip-sensitive); training should target family-specific failure modes rather than generic noise augmentation.

We will release our evaluation toolkit and complete results to support future research on building more robust VLMs.

Impact Statement

This work aims to improve robustness evaluation for vision-language models. We do not anticipate direct negative societal impacts from the benchmark itself; however, insights from robustness gaps can inform safer deployment and failure mitigation in real-world applications. We consider this research particularly useful for the development of foundation models for robotics that directly leverage VLMs as their backbones (e.g., (Intelligence et al., 2025; Goyal et al., 2025), inter alia). Because these embodied systems are heavily reliant on VLMs for high-level reasoning and perception, they inherently inherit the foundational weaknesses of their backbones. These vulnerabilities are often exacerbated in physical settings, where robots are routinely exposed to diverse visual perturbations and environmental corruptions—ranging from lighting shifts to sensor noise—that can compromise safety and operational reliability.

Acknowledgements

Rohit Saxena was supported by the Engineering and Physical Sciences Research Council (EPSRC) through the AI Hub in Generative Models (grant number EP/Y028805/1). Pasquale Minervini was partially funded by ELIAI (The Edinburgh Laboratory for Integrated Artificial Intelligence), EPSRC (grant no. EP/W002876/1), and a donation from Accenture LLP.

References

- Bai, S., Cai, Y., Chen, R., Chen, K., Chen, X., Cheng, Z., Deng, L., Ding, W., Gao, C., Ge, C., Ge, W., Guo, Z., Huang, Q., Huang, J., Huang, F., Hui, B., Jiang, S., Li, Z., Li, M., Li, M., Li, K., Lin, Z., Lin, J., Liu, X., Liu, J., Liu, C., Liu, Y., Liu, D., Liu, S., Lu, D., Luo, R., Lv, C., Men, R., Meng, L., Ren, X., Ren, X., Song, S., Sun, Y., Tang, J., Tu, J., Wan, J., Wang, P., Wang, P., Wang, Q., Wang, Y., Xie, T., Xu, Y., Xu, H., Xu, J., Yang, Z., Yang, M., Yang, J., Yang, A., Yu, B., Zhang, F., Zhang, H., Zhang, X., Zheng, B., Zhong, H., Zhou, J., Zhou, F., Zhou, J., Zhu, Y., and Zhu, K. Qwen3-vl technical report, 2025. URL <https://arxiv.org/abs/2511.21631>.
- Barbu, A., Mayo, D., Alverio, J., Luo, W., Wang, C., Gutfreund, D., Tenenbaum, J., and Katz, B. Objectnet: A large-scale bias-controlled dataset for pushing the limits of object recognition models. In Wallach, H., Larochelle, H., Beygelzimer, A., d'Alché-Buc, F., Fox, E., and Garnett, R. (eds.), *Advances in Neural Information Processing Systems*, volume 32. Curran Associates, Inc., 2019a. URL https://proceedings.neurips.cc/paper_files/paper/2019/file/97af07a14cacba681feacf3012730892-Paper.pdf.
- Barbu, A., Mayo, D., Alverio, J., Luo, W., Wang, C., Gutfreund, D., Tenenbaum, J., and Katz, B. Objectnet: A large-scale bias-controlled dataset for pushing the limits of object recognition models. In Wallach, H., Larochelle, H., Beygelzimer, A., d'Alché-Buc, F., Fox, E., and Garnett, R. (eds.), *Advances in Neural Information Processing Systems*, volume 32. Curran Associates, Inc., 2019b. URL https://proceedings.neurips.cc/paper_files/paper/2019/file/97af07a14cacba681feacf3012730892-Paper.pdf.
- Bhojanapalli, S., Chakrabarti, A., Glasner, D., Li, D., Unterthiner, T., and Veit, A. Understanding robustness of transformers for image classification. In *2021 IEEE/CVF International Conference on Computer Vision (ICCV)*, pp. 10211–10221, 2021. doi: 10.1109/ICCV48922.2021.01007.
- Carlini, N., Nasr, M., Choquette-Choo, C. A., Jagielski, M., Gao, I., Awadalla, A., Koh, P. W., Ippolito, D., Lee, K., Tramer, F., and Schmidt, L. Are aligned neural networks adversarially aligned? In *Proceedings of the 37th International Conference on Neural Information Processing Systems, NIPS '23*, Red Hook, NY, USA, 2023. Curran Associates Inc.
- Clark, C., Zhang, J., Ma, Z., Park, J. S., Salehi, M., Tripathi, R., Lee, S., Ren, Z., Kim, C. D., Yang, Y., Shao, V., Yang, Y., Huang, W., Gao, Z., Anderson, T., Zhang, J., Jain, J., Stoica, G., Han, W., Farhadi, A., and Krishna, R. Molmo2: Open weights and data for vision-language models with video understanding and grounding, 2026. URL <https://arxiv.org/abs/2601.10611>.
- Fan, Z., Wang, Y., Polisetty, S., and Fung, Y. R. Unveiling the lack of LVLM robustness to fundamental visual variations: Why and path forward. In Che, W., Nabende, J., Shutova, E., and Pilehvar, M. T. (eds.), *Findings of the Association for Computational Linguistics: ACL 2025*, pp. 20222–20242, Vienna, Austria, July 2025. Association for Computational Linguistics. ISBN 979-8-89176-256-5. doi: 10.18653/v1/2025.findings-acl.1037. URL <https://aclanthology.org/2025.findings-acl.1037/>.
- Fu, C., Chen, P., Shen, Y., Qin, Y., Zhang, M., Lin, X., Yang, J., Zheng, X., Li, K., Sun, X., Wu, Y., Ji, R., Shan, C., and He, R. Mme: A comprehensive evaluation benchmark for multimodal large language models, 2025. URL <https://arxiv.org/abs/2306.13394>.
- Goyal, A., Hadfield, H., Yang, X., Blukis, V., and Ramos, F. V1a-0: Building state-of-the-art vlms with zero modification. *arXiv preprint arXiv:2510.13054*, 2025.

- Hendrycks, D. and Dietterich, T. Benchmarking neural network robustness to common corruptions and perturbations. *Proceedings of the International Conference on Learning Representations*, 2019. URL <https://openreview.net/pdf?id=HJz6tiCqYm>.
- Hendrycks, D., Basart, S., Mu, N., Kadavath, S., Wang, F., Dorundo, E., Desai, R., Zhu, T., Parajuli, S., Guo, M., Song, D., Steinhardt, J., and Gilmer, J. The many faces of robustness: A critical analysis of out-of-distribution generalization. In *Proceedings of the IEEE/CVF International Conference on Computer Vision (ICCV)*, pp. 8340–8349, October 2021.
- Intelligence, P., Black, K., Brown, N., Darpinian, J., Dhabalia, K., Driess, D., Esmail, A., Equi, M., Finn, C., Fusai, N., Galliker, M. Y., Ghosh, D., Groom, L., Hausman, K., Ichter, B., Jakubczak, S., Jones, T., Ke, L., LeBlanc, D., Levine, S., Li-Bell, A., Mothukuri, M., Nair, S., Pertsch, K., Ren, A. Z., Shi, L. X., Smith, L., Springenberg, J. T., Stachowicz, K., Tanner, J., Vuong, Q., Walke, H., Walling, A., Wang, H., Yu, L., and Zhilinsky, U. $\pi_{0.5}$: a vision-language-action model with open-world generalization, 2025. URL <https://arxiv.org/abs/2504.16054>.
- Li, B., Lin, Z., Peng, W., Nyandwi, J. d. D., Jiang, D., Ma, Z., Khanuja, S., Krishna, R., Neubig, G., and Ramanan, D. Naturalbench: evaluating vision-language models on natural adversarial samples. In *Proceedings of the 38th International Conference on Neural Information Processing Systems, NIPS '24*, Red Hook, NY, USA, 2024. Curran Associates Inc. ISBN 9798331314385.
- Liu, J., Zeng, W., Zhang, X., Wang, Y., Shan, Z., and He, J. On the perception bottleneck of VLMs for chart understanding. In Christodoulopoulos, C., Chakraborty, T., Rose, C., and Peng, V. (eds.), *Findings of the Association for Computational Linguistics: EMNLP 2025*, pp. 10829–10841, Suzhou, China, November 2025. Association for Computational Linguistics. ISBN 979-8-89176-335-7. doi: 10.18653/v1/2025.findings-emnlp.573. URL <https://aclanthology.org/2025.findings-emnlp.573/>.
- Liu, Y., Duan, H., Zhang, Y., Li, B., Zhang, S., Zhao, W., Yuan, Y., Wang, J., He, C., Liu, Z., Chen, K., and Lin, D. Mmbench: Is your multi-modal model an all-around player? In *Computer Vision – ECCV 2024: 18th European Conference, Milan, Italy, September 29–October 4, 2024, Proceedings, Part VI*, pp. 216–233, Berlin, Heidelberg, 2024. Springer-Verlag. ISBN 978-3-031-72657-6. doi: 10.1007/978-3-031-72658-3_13. URL https://link.springer.com/chapter/10.1007/978-3-031-72658-3_13.
- Mao, C., Geng, S., Yang, J., Wang, X., and Vondrick, C. Understanding zero-shot adversarial robustness for large-scale models, 2023. URL <https://arxiv.org/abs/2212.07016>.
- McKinzie, B., Gan, Z., Fauconnier, J., Dodge, S., Zhang, B., Dufter, P., Shah, D., Du, X., Peng, F., Belyi, A., Zhang, H., Singh, K., Kang, D., Hè, H., Schwarzer, M., Gunter, T., Kong, X., Zhang, A., Wang, J., Wang, C., Du, N., Lei, T., Wiseman, S., Lee, M., Wang, Z., Pang, R., Gräsch, P., Toshev, A., and Yang, Y. MM1: methods, analysis and insights from multimodal LLM pre-training. In *ECCV (29)*, volume 15087 of *Lecture Notes in Computer Science*, pp. 304–323. Springer, 2024.
- Paul, S. and Chen, P. Vision transformers are robust learners. In *Thirty-Sixth AAAI Conference on Artificial Intelligence, AAAI 2022, Thirty-Fourth Conference on Innovative Applications of Artificial Intelligence, IAAI 2022, The Twelfth Symposium on Educational Advances in Artificial Intelligence, EAAI 2022 Virtual Event, February 22 - March 1, 2022*, pp. 2071–2081. AAAI Press, 2022. doi: 10.1609/AAAI.V36I2.20103. URL <https://doi.org/10.1609/aaai.v36i2.20103>.
- Qi, X., Huang, K., Panda, A., Henderson, P., Wang, M., and Mittal, P. Visual adversarial examples jailbreak aligned large language models. In *Proceedings of the Thirty-Eighth AAAI Conference on Artificial Intelligence and Thirty-Sixth Conference on Innovative Applications of Artificial Intelligence and Fourteenth Symposium on Educational Advances in Artificial Intelligence, AAAI'24/IAAI'24/EAAI'24*. AAAI Press, 2024. ISBN 978-1-57735-887-9. doi: 10.1609/aaai.v38i19.30150. URL <https://doi.org/10.1609/aaai.v38i19.30150>.
- Sellergren, A., Kazemzadeh, S., Jaroensri, T., Kiraly, A., Traverse, M., Kohlberger, T., Xu, S., Jamil, F., Hughes, C., Lau, C., Chen, J., Mahvar, F., Yatziv, L., Chen, T., Sterling, B., Baby, S. A., Baby, S. M., Lai, J., Schmidgall, S., Yang, L., Chen, K., Bjornsson, P., Reddy, S., Brush, R., Philbrick, K., Asiedu, M., Mezerreg, I., Hu, H., Yang, H., Tiwari, R., Jansen, S., Singh, P., Liu, Y., Azizi, S., Kamath, A., Ferret, J., Pathak, S., Vieillard, N., Merhej, R., Perrin, S., Matejovicova, T., Ramé, A., Riviere, M., Rouillard, L., Mesnard, T., Cideron, G., bastien Grill, J., Ramos, S., Yvinec, E., Casbon, M., Buchatskaya, E., Alayrac, J.-B., Lepikhin, D., Feinberg, V., Borgeaud, S., Andreev, A., Hardin, C., Dadashi, R., Hussenot, L., Joulain, A., Bachem, O., Matias, Y., Chou, K., Hassidim, A., Goel, K., Farabet, C., Barral, J., Warkentin, T., Shlens, J., Fleet, D., Cotruta, V., Sanseviero, O., Martins, G., Kirk, P., Rao, A., Shetty, S., Steiner, D. F., Kirmizibayrak, C., Pilgrim, R., Golden, D., and Yang, L. Medgemma

- technical report, 2025. URL <https://arxiv.org/abs/2507.05201>.
- Shayegani, E., Dong, Y., and Abu-Ghazaleh, N. B. Jailbreak in pieces: Compositional adversarial attacks on multi-modal language models. In *The Twelfth International Conference on Learning Representations, ICLR 2024, Vienna, Austria, May 7-11, 2024*. OpenReview.net, 2024. URL <https://openreview.net/forum?id=plmBsXHxgR>.
- Team, G., Kamath, A., Ferret, J., Pathak, S., Vieillard, N., Merhej, R., Perrin, S., Matejovicova, T., Ramé, A., Rivière, M., Rouillard, L., Mesnard, T., Cideron, G., bastien Grill, J., Ramos, S., Yvinec, E., Casbon, M., Pot, E., Penchev, I., Liu, G., Visin, F., Kenealy, K., Beyer, L., Zhai, X., Tsitsulin, A., Busa-Fekete, R., Feng, A., Sachdeva, N., Coleman, B., Gao, Y., Mustafa, B., Barr, I., Parisotto, E., Tian, D., Eyal, M., Cherry, C., Peter, J.-T., Sinopalnikov, D., Bhupatiraju, S., Agarwal, R., Kazemi, M., Malkin, D., Kumar, R., Vilar, D., Brusilovsky, I., Luo, J., Steiner, A., Friesen, A., Sharma, A., Sharma, A., Gilady, A. M., Goedeckemeyer, A., Saade, A., Feng, A., Kolesnikov, A., Bendebury, A., Abdagic, A., Vadi, A., György, A., Pinto, A. S., Das, A., Bapna, A., Miech, A., Yang, A., Paterson, A., Shenoy, A., Chakrabarti, A., Piot, B., Wu, B., Shahriari, B., Petrini, B., Chen, C., Lan, C. L., Choquette-Choo, C. A., Carey, C., Brick, C., Deutsch, D., Eisenbud, D., Cattle, D., Cheng, D., Paparas, D., Sreepathihalli, D. S., Reid, D., Tran, D., Zelle, D., Noland, E., Huizenga, E., Kharitonov, E., Liu, F., Amirkhanyan, G., Cameron, G., Hashemi, H., Klimczak-Plucińska, H., Singh, H., Mehta, H., Lehri, H. T., Hazimeh, H., Ballantyne, I., Szpektor, I., Nardini, I., Pouget-Abadie, J., Chan, J., Stanton, J., Wieting, J., Lai, J., Orbay, J., Fernandez, J., Newlan, J., yeong Ji, J., Singh, J., Black, K., Yu, K., Hui, K., Vodrahalli, K., Greff, K., Qiu, L., Valentine, M., Coelho, M., Ritter, M., Hoffman, M., Watson, M., Chaturvedi, M., Moynihan, M., Ma, M., Babar, N., Noy, N., Byrd, N., Roy, N., Momchev, N., Chauhan, N., Sachdeva, N., Bunyan, O., Botarda, P., Caron, P., Rubenstein, P. K., Culliton, P., Schmid, P., Sessa, P. G., Xu, P., Stanczyk, P., Tafti, P., Shivanna, R., Wu, R., Pan, R., Rokni, R., Willoughby, R., Vallu, R., Mullins, R., Jerome, S., Smoot, S., Girgin, S., Iqbal, S., Reddy, S., Sheth, S., Pöder, S., Bhatnagar, S., Panyam, S. R., Eiger, S., Zhang, S., Liu, T., Yacovone, T., Liechty, T., Kalra, U., Evci, U., Misra, V., Roseberry, V., Feinberg, V., Kolesnikov, V., Han, W., Kwon, W., Chen, X., Chow, Y., Zhu, Y., Wei, Z., Egyed, Z., Cotruta, V., Giang, M., Kirk, P., Rao, A., Black, K., Babar, N., Lo, J., Moreira, E., Martins, L. G., Sanseviero, O., Gonzalez, L., Gleicher, Z., Warkentin, T., Mirrokni, V., Senter, E., Collins, E., Barral, J., Ghahramani, Z., Hadsell, R., Matias, Y., Sculley, D., Petrov, S., Fiedel, N., Shazeer, N., Vinyals, O., Dean, J., Hassabis, D., Kavukcuoglu, K., Farabet, C., Buchatskaya, E., Alayrac, J.-B., Anil, R., Dmitry, Lepikhin, Borgeaud, S., Bachem, O., Joulin, A., Andreev, A., Hardin, C., Dadashi, R., and Hussenot, L. Gemma 3 technical report, 2025. URL <https://arxiv.org/abs/2503.19786>.
- Tong, S., Liu, Z., Zhai, Y., Ma, Y., LeCun, Y., and Xie, S. Eyes wide shut? exploring the visual shortcomings of multimodal llms. In *IEEE/CVF Conference on Computer Vision and Pattern Recognition, CVPR 2024, Seattle, WA, USA, June 16-22, 2024*, pp. 9568–9578. IEEE, 2024. doi: 10.1109/CVPR52733.2024.00914. URL <https://doi.org/10.1109/CVPR52733.2024.00914>.
- Usama, M., Asim, S. A., Ali, S. B., Wasim, S. T., and Mansoor, U. B. Analysing the robustness of vision-language-models to common corruptions, 2025. URL <https://arxiv.org/abs/2504.13690>.
- Wang, W., Gao, Z., Gu, L., Pu, H., Cui, L., Wei, X., Liu, Z., Jing, L., Ye, S., Shao, J., Wang, Z., Chen, Z., Zhang, H., Yang, G., Wang, H., Wei, Q., Yin, J., Li, W., Cui, E., Chen, G., Ding, Z., Tian, C., Wu, Z., Xie, J., Li, Z., Yang, B., Duan, Y., Wang, X., Hou, Z., Hao, H., Zhang, T., Li, S., Zhao, X., Duan, H., Deng, N., Fu, B., He, Y., Wang, Y., He, C., Shi, B., He, J., Xiong, Y., Lv, H., Wu, L., Shao, W., Zhang, K., Deng, H., Qi, B., Ge, J., Guo, Q., Zhang, W., Zhang, S., Cao, M., Lin, J., Tang, K., Gao, J., Huang, H., Gu, Y., Lyu, C., Tang, H., Wang, R., Lv, H., Ouyang, W., Wang, L., Dou, M., Zhu, X., Lu, T., Lin, D., Dai, J., Su, W., Zhou, B., Chen, K., Qiao, Y., Wang, W., and Luo, G. Internvl3.5: Advancing open-source multimodal models in versatility, reasoning, and efficiency, 2025a. URL <https://arxiv.org/abs/2508.18265>.
- Wang, Z., Yu, W., REN, X., Zhang, J., Zhao, Y., Saxena, R., Cheng, L., Wong, G., See, S., Minervini, P., Song, Y., and Steedman, M. MMLongbench: Benchmarking long-context vision-language models effectively and thoroughly. In *ICML 2025 Workshop on Long-Context Foundation Models, 2025b*. URL <https://openreview.net/forum?id=zsdJSkeS9S>.
- Ye, J., Wu, Y., Gao, S., Huang, C., Li, S., Li, G., Fan, X., Zhang, Q., Gui, T., and Huang, X. RoTBench: A multi-level benchmark for evaluating the robustness of large language models in tool learning. In Al-Onaizan, Y., Bansal, M., and Chen, Y.-N. (eds.), *Proceedings of the 2024 Conference on Empirical Methods in Natural Language Processing*, pp. 313–333, Miami, Florida, USA, November 2024. Association for Computational Linguistics. doi: 10.18653/v1/2024.emnlp-main.19. URL <https://aclanthology.org/2024.emnlp-main.19/>.

- Yu, H., Liu, J., Zhang, X., Wu, J., and Cui, P. A survey on evaluation of out-of-distribution generalization, 2024. URL <https://arxiv.org/abs/2403.01874>.
- Yue, X., Ni, Y., Zheng, T., Zhang, K., Liu, R., Zhang, G., Stevens, S., Jiang, D., Ren, W., Sun, Y., Wei, C., Yu, B., Yuan, R., Sun, R., Yin, M., Zheng, B., Yang, Z., Liu, Y., Huang, W., Sun, H., Su, Y., and Chen, W. MMMU: A massive multi-discipline multimodal understanding and reasoning benchmark for expert AGI. In *IEEE/CVF Conference on Computer Vision and Pattern Recognition, CVPR 2024, Seattle, WA, USA, June 16-22, 2024*, pp. 9556–9567. IEEE, 2024. doi: 10.1109/CVPR52733.2024.00913. URL <https://doi.org/10.1109/CVPR52733.2024.00913>.
- Yue, X., Zheng, T., Ni, Y., Wang, Y., Zhang, K., Tong, S., Sun, Y., Yu, B., Zhang, G., Sun, H., Su, Y., Chen, W., and Neubig, G. MMMU-pro: A more robust multi-discipline multimodal understanding benchmark. In Che, W., Nabende, J., Shutova, E., and Pilehvar, M. T. (eds.), *Proceedings of the 63rd Annual Meeting of the Association for Computational Linguistics (Volume 1: Long Papers)*, pp. 15134–15186, Vienna, Austria, July 2025. Association for Computational Linguistics. ISBN 979-8-89176-251-0. doi: 10.18653/v1/2025.acl-long.736. URL <https://aclanthology.org/2025.acl-long.736/>.
- Zhao, Y., Pang, T., Du, C., Yang, X., Li, C., Cheung, N.-M., and Lin, M. On evaluating adversarial robustness of large vision-language models. In *Proceedings of the 37th International Conference on Neural Information Processing Systems, NIPS '23, Red Hook, NY, USA, 2023*. Curran Associates Inc.
- Zhou, C., Wang, M., Ma, Y., Wu, C., Chen, W., Qian, Z., Liu, X., Zhang, Y., Wang, J., Xu, H., Luo, F., Chen, X., Hao, X., Li, H., Zhang, A., Wang, W., Zhang, K., Jia, G., Li, L., Lu, Z., Lu, Y., and Guo, Y. From perception to cognition: A survey of vision-language interactive reasoning in multimodal large language models, 2025. URL <https://arxiv.org/abs/2509.25373>.
- Zhou, D., Yu, Z., Xie, E., Xiao, C., Anandkumar, A., Feng, J., and Alvarez, J. M. Understanding the robustness in vision transformers. In Chaudhuri, K., Jegelka, S., Song, L., Szepesvari, C., Niu, G., and Sabato, S. (eds.), *Proceedings of the 39th International Conference on Machine Learning*, volume 162 of *Proceedings of Machine Learning Research*, pp. 27378–27394. PMLR, 17–23 Jul 2022. URL <https://proceedings.mlr.press/v162/zhou22m.html>.
- Zhou, X., Liu, M., Yurtsever, E., Zagar, B. L., Zimmer, W., Cao, H., and Knoll, A. C. Vision language models in autonomous driving: A survey and outlook. *IEEE Transactions on Intelligent Vehicles*, pp. 1–20, 2024. doi: 10.1109/TIV.2024.3402136.

Model	MMBench worst (aug, level, drop)	MMMU-Pro worst (aug, level, drop)
Qwen3-VL-4B	upsample (high, 26.3)	elastic_transform (high, 7.4)
Qwen3-VL-8B	upsample (high, 30.2)	elastic_transform (high, 8.9)
Qwen3-VL-30B	upsample (high, 29.4)	elastic_transform (high, 13.9)
InternVL3.5-4B	upsample (high, 30.6)	zoom_blur (high, 11.1)
InternVL3.5-8B	upsample (high, 31.6)	zoom_blur (high, 12.3)
InternVL3.5-14B	upsample (high, 29.4)	zoom_blur (high, 9.6)
Molmo2-4B	upsample (high, 33.1)	upsample (high, 5.6)
Molmo2-8B	upsample (high, 33.9)	upsample (high, 5.6)
Gemma-3-12B	upsample (high, 32.1)	upsample (high, 9.9)
Qwen3-VL-4B-Thinking	upsample (high, 29.5)	upsample (mid, 19.1)
Qwen3-VL-8B-Thinking	upsample (high, 30.8)	upsample (high, 23.1)

Table 7. Worst-case augmentation per model. Drop is baseline minus accuracy under that augmentation (percentage points); “bin” denotes binary augmentations.

Category	MMBench		MMMU-Pro	
	Drop	Subject	Drop	Subject
image_style	5.30	Art	4.75	
attribute_comparison	5.26	Music	3.90	
structuralized_imagetext_understanding	4.81	Economics	3.69	
social_relation	4.57	Art_Theory	3.46	
nature_relation	4.51	Pharmacy	3.35	

Table 8. Top-5 dataset categories with the largest average drops (percentage points), aggregated across models in direct mode.

A. Additional Results

A.1. Worst-Case Augmentations

A.2. Dataset Category Sensitivity

A.3. Scaling Trends

A.4. Prompting-Mode Performance (Qwen)

A.5. Prompting-Mode Tier Distributions (Qwen)

A.6. Positive Augmentations

A small number of augmentations yield negative Δ (i.e., higher accuracy than baseline). On MMBench, `brightness:low/mid`, `gamma_up:low/mid`, and `gaussian_noise:low` show marginal gains (-0.1 to -0.2 pp); on MMMU-Pro, `hue_shift:low`, `gaussian_blur:low`, and `speckle_noise:low/mid` exhibit similar small effects. Given the magnitude (<0.5 pp), these may reflect noise, mild regularization, or dataset-specific priors rather than robust improvements; we note them for completeness but do not draw strong conclusions.

A.7. Family-Level Vulnerability Matrix

A.8. Per-Model Top-5 Corruptions

Tables 13 and 14 provide per-model top-5 most harmful corruptions at each severity. The aggregate patterns from Figure 2 hold consistently across models: `glass_blur` dominates at low severity, while `upsample` and `elastic_transform` dominate at mid/high severities.

Family	MMMU-Pro slope (R^2 , n)	MMBench slope (R^2 , n)
Qwen3-VL	+2.95 (1.00, n=3)	-0.38 (0.17, n=3)
InternVL3.5	-0.94 (0.12, n=3)	-1.44 (0.89, n=3)
Molmo2	-1.66 (1.00, n=2)	-1.00 (1.00, n=2)

Table 9. Scaling of robustness drop with model size within families (direct mode). Slope is the change in drop per $\log_{10}(\text{parameters})$; negative values indicate improved robustness with scale.

Model	MMMU-Pro		MMBench	
	Baseline	Drop	Baseline	Drop
Qwen3-VL-4B-COT	32.1	+1.3	86.9	+2.5
Qwen3-VL-8B-COT	42.0	+3.1	89.6	+3.2
Qwen3-VL-4B-Thinking	43.5	+2.5	89.3	+1.8
Qwen3-VL-8B-Thinking	50.0	+3.8	91.1	+3.0

Table 10. Baseline accuracy and mean drop for Qwen models under COT and thinking modes. Drop is averaged over the 133 corrupted configurations. Direct-mode results are in Table 3.

Mode	Mild	Moderate	Catastrophic	Positive
MMBench (Qwen models)				
Direct	23.6	17.0	3.5	21.6
COT	28.9	23.3	5.6	16.9
Thinking	27.1	21.1	4.1	16.2
MMMU-Pro (Qwen models)				
Direct	19.8	10.3	1.3	42.1
COT	19.5	21.4	6.4	26.7
Thinking	18.8	19.9	13.2	27.8

Table 11. Tier shares (%) for Qwen models by prompting mode.

Aug-Sev	Gemma	Qwen	InternVL	Molmo
shot_noise:high	12.90	5.12	12.39	5.62
pixelate:high	11.37	6.06	12.97	8.27
downsample:high	8.79	4.92	9.73	6.74
solarize:high	10.08	9.03	12.93	8.50

Table 12. Family-level mean drops (MMBench, direct) for selected aug-level pairs.

Model	Low	Mid	High
Gemma3-12B	glass_blur	(10.7),	upsample (15.2),
	solarize	(3.6),	shot_noise (8.4),
	shot_noise	(2.5),	glass_blur (8.2),
	upsample	(2.5),	elastic_transform (6.7),
	text_overlay (2.3)		zoom_blur (6.0)
InternVL3.5-4B	glass_blur	(10.7),	upsample (17.6),
	solarize	(7.3),	glass_blur (9.6),
	upsample	(3.9),	elastic_transform (8.6),
	shot_noise	(3.2),	solarize (7.3),
	zoom_blur (2.3)		zoom_blur (7.3)
InternVL3.5-8B	glass_blur	(9.3),	upsample (17.1),
	solarize	(8.1),	elastic_transform (8.7),
	upsample	(4.5),	zoom_blur (8.0),
	shot_noise	(3.4),	glass_blur (7.4),
	grid_mask (2.8)		solarize (7.3)
InternVL3.5-14B	glass_blur	(9.5),	upsample (17.9),
	solarize	(5.3),	glass_blur (7.8),
	shot_noise	(3.3),	elastic_transform (6.6),
	upsample	(3.2),	zoom_blur (6.5),
	grid_mask (1.1)		solarize (5.5)
Molmo2-4B	glass_blur	(7.4),	upsample (15.9),
	solarize	(5.5),	zoom_blur (6.3),
	upsample	(4.1),	glass_blur (5.7),
	shot_noise	(2.1),	elastic_transform (4.9),
	grid_mask (1.9)		solarize (4.3)
Molmo2-8B	glass_blur	(6.3),	upsample (18.9),
	solarize	(4.6),	glass_blur (6.7),
	upsample	(3.5),	elastic_transform (6.6),
	grid_mask	(1.1),	zoom_blur (4.5),
	zoom_blur (0.6)		solarize (4.3)
Qwen3-VL-4B	glass_blur	(7.0),	upsample (13.1),
	solarize	(4.5),	elastic_transform (5.7),
	upsample	(2.6),	glass_blur (5.4),
	random_occlusion	(1.2),	zoom_blur (4.5),
	elastic_transform (1.1)		solarize (4.1)
Qwen3-VL-8B	glass_blur	(8.2),	upsample (14.2),
	solarize	(5.9),	glass_blur (7.0),
	grid_mask	(2.3),	elastic_transform (6.1),
	shot_noise	(1.8),	solarize (6.0),
	upsample (1.8)		zoom_blur (5.2)
Qwen3-VL-30B	solarize	(6.1),	upsample (11.8),
	glass_blur	(5.6),	elastic_transform (6.2),
	upsample	(2.6),	solarize (4.9),
	random_occlusion	(1.2),	glass_blur (4.3),
	watermark (1.1)		zoom_blur (4.3)

Table 13. Per-model top-5 most harmful corruptions at each severity (MMBench, direct mode). Values are accuracy drops in percentage points.

Model	Low	Mid	High
Gemma3-12B	glass_blur	(8.9),	upsample (9.6),
	solarize	(4.9),	zoom_blur (8.9),
	brightness	(3.7),	elastic_transform (5.2),
	grid_mask	(3.7),	glass_blur (4.6),
	defocus_blur (3.4)		motion_blur (4.6)
InternVL3.5-4B	glass_blur	(5.6),	upsample (9.6),
	upsample	(5.6),	upsample (6.5),
	grid_mask	(3.7),	glass_blur (5.2),
	solarize	(3.1),	grid_mask (4.9),
	watermark (2.5)		elastic_transform (4.6)
InternVL3.5-8B	glass_blur	(5.6),	zoom_blur (11.7),
	zoom_blur	(4.6),	upsample (8.0),
	grid_mask	(4.3),	random_occlusion (4.9),
	motion_blur	(3.7),	glass_blur (4.6),
	rotate (2.8)		motion_blur (4.6)
InternVL3.5-14B	glass_blur	(5.9),	zoom_blur (8.3),
	upsample (3.4), snow	(1.5),	upsample (7.4),
	zoom_blur	(1.5),	glass_blur (5.2), rotate (2.8),
	grid_mask (1.2)		grid_mask (2.5)
Molmo2-4B	glass_blur (4.3), rotate	(1.5),	upsample (4.3),
	shot_noise	(1.2),	glass_blur (3.1),
	addborder	(0.9),	zoom_blur (3.1),
	brightness_up (0.9)		brightness_up (1.9),
Molmo2-8B	glass_blur	(4.0),	upsample (3.7),
	zoom_blur	(1.9),	zoom_blur (3.7),
	upsample	(1.5),	elastic_transform (2.5),
	center_occlusion	(1.2),	rotate (2.5), glass_blur (2.2)
Qwen3-VL-4B	gamma_up (0.6)		gamma_up (1.9)
	glass_blur	(2.8),	upsample (5.2),
	upsample (1.5), gamma	(0.6),	zoom_blur (5.2),
	saturation	(0.3),	glass_blur (2.2),
Qwen3-VL-8B	sharpen (0.0)		solarize (1.5),
	glass_blur	(5.2),	downsample (0.9)
	watermark	(2.8),	zoom_blur (8.0),
	upsample	(2.2),	upsample (7.4),
Qwen3-VL-30B	salt_pepper (1.2), snow	(1.2)	watermark (4.0),
	glass_blur	(6.8),	glass_blur (3.7),
	upsample	(6.2),	elastic_transform (2.2)
	grid_mask (3.7), affine	(2.8),	upsample (12.0),
Qwen3-VL-30B	watermark (2.8)		elastic_transform (6.2),
	glass_blur	(6.8),	zoom_blur (12.0),
	upsample	(6.2),	zoom_blur (13.9),
	grid_mask (3.7), affine	(2.8),	upsample (12.7),
Qwen3-VL-30B	watermark (2.8)		glass_blur (5.2),
	glass_blur	(6.8),	grid_mask (7.4),
	upsample	(6.2),	grid_mask (4.9)
	grid_mask (3.7), affine	(2.8),	pixelate (6.5)

Table 14. Per-model top-5 most harmful corruptions at each severity (MMM-U-Pro, direct mode). Values are accuracy drops in percentage points.

A.9. Detailed Robustness Results by Family

We provide the complete breakdown of accuracy drops for key augmentation types across the four model families. Values represent the family-averaged drop (percentage points) at Low, Mid, and High severity on MMBench.

Table 15. **Qwen3-VL Family:** Mean accuracy drops on MMBench. Note the resilience to noise (e.g., Gaussian Noise) vs. fragility to resampling (Upsample).

Augmentation	Low	Mid	High
Upsample	2.31	13.05	28.65
Elastic Transform	0.78	6.02	25.32
Zoom Blur	0.55	4.65	10.94
Solarize	5.47	5.00	9.03
Glass Blur	6.96	5.59	4.10
Pixelate	0.16	0.35	6.06
Shot Noise	0.55	2.19	5.12
Brightness	0.23	0.23	3.99
JPEG Compression	0.20	0.27	0.31

Table 16. **InternVL3.5 Family:** Mean accuracy drops on MMBench. This family shows higher sensitivity to pixelation and noise compared to Qwen.

Augmentation	Low	Mid	High
Upsample	3.83	17.55	30.56
Elastic Transform	0.78	7.94	26.30
Zoom Blur	1.60	7.23	13.36
Pixelate	0.55	1.60	12.97
Solarize	6.88	6.68	12.93
Shot Noise	3.28	5.98	12.39
Glass Blur	9.81	8.28	7.11
Motion Blur	0.74	3.05	7.31
JPEG Compression	0.20	0.27	0.63

Table 17. **Gemma 3 & Molmo 2 Families:** Comparison of key failure modes (High Severity Drops).

Augmentation (High)	Gemma 3 (12B)	Molmo 2 (Avg)
Upsample	32.12	33.47
Elastic Transform	23.45	24.74
Zoom Blur	13.25	9.67
Shot Noise	12.90	5.62
Pixelate	11.37	8.26
Solarize	10.08	8.50
Glass Blur	5.51	6.10

A.10. Tier Distributions

Table 18 reports tier distributions by severity level (direct mode, 9 models \times 42 severity-based augmentations per level, plus 9×7 binary).

Table 19 breaks down tier shares per model, highlighting that catastrophic and positive rates vary widely even within families.

A.11. RCE by Severity

Table 20 reports mean RCE across models by severity level. Higher RCE on MMMU-Pro reflects its smaller Visual Gain denominator. Two configurations on MMMU-Pro exceed 100% RCE (`upsample:high` and `elastic_transform:high` for Qwen3-VL-4B), indicating truly adversarial corruptions.

Dataset	Severity	Benign	Mild	Moderate	Catastrophic
MMBench	Low	304	48	24	2
	Mid	182	127	60	9
	High	94	113	133	38
	Binary	9	12	33	9
MMMU-Pro	Low	276	77	25	0
	Mid	230	93	52	3
	High	188	105	79	6
	Binary	37	15	11	0

Table 18. Tier distribution by severity level (counts out of 378 for severity-based, 63 for binary). Tiers use fixed thresholds: Catastrophic = $\Delta > 10pp$. Binary augmentations on MMBench produce 9 catastrophic cases—matching mid-severity—driven by vertical flip and color inversion.

MMBench (Direct)				
Model	Mild %	Moderate %	Catastrophic Rate (%)	Positive %
Qwen3-VL-4B	21.8	18.0	2.3	24.1
Qwen3-VL-8B	28.6	19.5	4.5	11.3
Qwen3-VL-30B	18.0	13.5	3.8	29.3
InternVL3.5-4B	29.3	30.1	8.3	3.8
InternVL3.5-8B	26.3	28.6	6.8	11.3
InternVL3.5-14B	18.0	21.1	6.8	14.3
Molmo2-4B	27.1	21.1	2.3	8.3
Molmo2-8B	21.1	17.3	2.3	17.3
Gemma-3-12B	35.3	18.8	6.8	6.0

MMMU-Pro (Direct)				
Model	Mild %	Moderate %	Catastrophic Rate (%)	Positive %
Qwen3-VL-4B	9.0	3.8	0.0	74.4
Qwen3-VL-8B	15.0	7.5	0.0	39.8
Qwen3-VL-30B	35.3	19.5	3.8	12.0
InternVL3.5-4B	24.8	16.5	0.8	26.3
InternVL3.5-8B	38.3	24.8	2.3	6.0
InternVL3.5-14B	17.3	10.5	0.0	37.6
Molmo2-4B	15.8	5.3	0.0	19.5
Molmo2-8B	12.8	5.3	0.0	51.1
Gemma-3-12B	49.6	32.3	0.0	3.0

Table 19. Per-model tier shares (%) across 133 augmentation configurations (direct mode). Tiers use fixed thresholds: Catastrophic = $\Delta > 10pp$ (distinct from the relative Severe-Failure Rate in Table 3). Benign shares are omitted for brevity.

A.12. Per-Example Flip Decomposition

Table 21 shows answer-flip rates (fraction of questions correct on clean that become incorrect under corruption) for a representative model (Qwen3-VL-8B) on MMBench. Spatial/resampling corruptions cause substantially more flips than photometric ones, even when the latter are at high severity.

Accuracy drop Δ conflates two opposing effects: examples the model previously answered correctly but now fails (*harmful flips*, Flip^+), and examples it previously failed but now succeeds (*helpful flips*, Flip^-):

$$\text{Flip}^+ = \Pr(\text{correct}_{\text{clean}} \wedge \text{wrong}_{\text{corrupted}}) \tag{5}$$

$$\text{Flip}^- = \Pr(\text{wrong}_{\text{clean}} \wedge \text{correct}_{\text{corrupted}}) \tag{6}$$

with net accuracy drop $\Delta = \text{Flip}^+ - \text{Flip}^-$. Flip rates are computed per example then averaged across the dataset; when aggregating across models or corruptions, we report macro-averages. This decomposition reveals whether drops stem from genuine failures or are partially masked by compensating gains.

Dataset	Severity	Mean RCE (%)	Interpretation
MMBench	Low	1.6	Minimal visual loss
	Mid	4.0	Moderate impact
	High	9.7	~10% visual loss
	Binary	11.5	Highest relative harm
MMMU-Pro	Low	2.7	Low but > MMBench
	Mid	6.3	Moderate
	High	13.0	Severe relative loss
	Binary	10.1	High relative harm

Table 20. Mean Relative Corruption Error by severity. RCE measures what fraction of visual contribution is destroyed. Higher RCE on MMMU-Pro reflects its smaller Visual Gain denominator.

Corruption	Severity	Flip rate
glass_blur	low	11.7%
upsample	high	36.3%
elastic_transform	high	32.9%
brightness	high	4.4%
jpeg_compression	high	1.6%

Table 21. Answer-flip rates for Qwen3-VL-8B on MMBench. Spatial/resampling corruptions (top) cause substantially more flips than photometric ones (bottom), even at high severity.

Flip Rates by Severity. Table 22 reports flip rates aggregated by severity level. On MMBench, harmful flips escalate sharply (1.8% at low \rightarrow 6.3% at high), while helpful flips remain low (1.1–1.8%), confirming that accuracy drops reflect genuine failures rather than noise. Binary augmentations show the highest harmful flip rate (12.3%)—over 6 \times the low-severity rate—with minimal compensation (1.6% Flip⁻). For severity-based corruptions, MMMU-Pro exhibits smaller Flip⁺/Flip⁻ ratios (1.2–1.6 \times vs. 1.7–3.6 \times on MMBench), consistent with its lower visual reliance.

Model-Specific Patterns. Table 23 reveals striking model differences. On MMBench, Molmo2 models exhibit the highest Flip⁺/Flip⁻ ratios (3.9–4.2), indicating “clean” degradation with minimal lucky compensations. Gemma-3-12B and InternVL3.5 models have the highest absolute Flip⁺ rates (5.1–5.5%), making them the most fragile. On MMMU-Pro, Qwen3-VL-4B achieves a ratio below 1.0 (0.85), meaning corruptions *help more than hurt*—strong evidence of minimal visual reliance on reasoning tasks.

Binary Augmentation Flips. Table 24 drills into per-augmentation flip rates for binary transforms. On MMBench, `flip_v` and `invert` consistently cause 10–15% harmful flips across models, with InternVL3.5-4B reaching 15.7% for vertical flip. On MMMU-Pro, the same augmentations show dramatically lower Flip⁺ (5–11%) and higher Flip⁻, with some models (Molmo2-8B) showing near-zero or negative net flips for `flip_h`—confirming that spatial transforms harm perception far more than reasoning.

A.13. Answer-Flip Rates Across Models

Table 25 extends the flip-rate analysis to all direct-mode models for selected corruptions. Flip rate is defined as the fraction of questions answered correctly on clean images that become incorrect under corruption.

Dataset	Severity	Flip ⁺ (%)	Flip ⁻ (%)	Ratio
MMBench	Low	1.79	1.05	1.70
	Mid	3.37	1.49	2.26
	High	6.33	1.78	3.56
	Binary	12.27	1.63	7.53
MMMUPro	Low	2.16	1.74	1.24
	Mid	3.20	2.31	1.39
	High	4.47	2.82	1.59
	Binary	5.30	2.65	2.00

Table 22. Flip rates by severity level (averaged over models). Flip⁺ = harmful (correct→wrong), Flip⁻ = helpful (wrong→correct). Higher ratios indicate “purer” degradation with less compensating gains.

Model	MMBench		MMMUPro	
	Flip ⁺	Ratio	Flip ⁺	Ratio
Qwen3-VL-4B	3.69	2.55	2.37	0.85
Qwen3-VL-8B	4.46	2.76	3.64	1.21
Qwen3-VL-30B	3.72	2.20	4.16	2.08
InternVL3.5-4B	5.13	3.79	3.42	1.79
InternVL3.5-8B	5.27	3.27	3.93	2.74
InternVL3.5-14B	4.45	3.01	2.94	1.44
Molmo2-4B	3.63	3.94	2.75	1.32
Molmo2-8B	3.24	4.19	2.50	1.06
Gemma-3-12B	5.53	2.31	5.13	2.19

Table 23. Model flip rates (%) and Flip⁺/Flip⁻ ratios. Higher ratios indicate purer degradation. Bold: highest Flip⁺ (most fragile) and extreme ratios.

Augmentation	MMBench			MMMUPro		
	Flip ⁺	Flip ⁻	Net	Flip ⁺	Flip ⁻	Net
flip_v	12.4	2.0	10.4	8.3	4.1	4.2
flip_h	9.0	1.9	7.1	7.2	3.6	3.6
invert	12.1	1.7	10.4	3.7	2.4	1.3
channel_swap	4.5	1.2	3.3	1.1	1.2	-0.1
equalize	5.1	1.6	3.5	2.7	2.6	0.1
grayscale	4.6	1.5	3.2	1.8	1.5	0.3
autocontrast	0.2	0.2	0.0	0.3	0.6	-0.2

Table 24. Binary augmentation flip rates (%) averaged over 9 direct-mode models. Vertical flip and invert dominate harmful flips on MMBench but show reduced impact on MMMUPro.

Model	glass:low	ups:high	elast:high	bright:high	jpeg:high
Qwen3-VL-4B	8.4	29.2	29.1	2.7	1.4
Qwen3-VL-8B	10.6	32.4	29.1	4.0	1.4
Qwen3-VL-30B	8.6	31.2	26.7	2.5	1.5
InternVL3.5-4B	12.8	33.2	27.9	4.8	2.3
InternVL3.5-8B	12.4	34.7	32.0	5.5	1.9
InternVL3.5-14B	12.2	32.4	27.2	3.9	1.4
Molmo2-4B	9.0	34.7	26.4	3.9	0.8
Molmo2-8B	7.9	35.4	27.1	3.8	1.1
Gemma3-12B	14.2	35.8	26.6	6.6	4.3

Table 25. Answer-flip rates (%) across 9 direct-mode models on MMBench. Spatial/resampling corruptions (columns 2–4) consistently cause higher flip rates than photometric ones (columns 5–6). Thinking models are excluded due to different output format.

B. Quantitative Robustness Metrics

B.1. Severity Mismatch Metrics

Table 26 reports the consistency between visual severity levels and model performance drops. A high violation rate indicates that increasing visual severity does not reliably lead to larger performance drops.

Table 26. Severity mismatch metrics. **Violation Rate**: Fraction of augmentation trajectories where drop does not strictly increase with severity. **Mean Spearman ρ** : Rank correlation between severity and drop (averaged across models/augmentations).

Dataset	Violation Rate (%)	Mean Spearman ρ
MMBench	30.2	0.71
MMMU-Pro	56.1	0.34

B.2. Tail Risk Share from Spatial/Resampling Corruptions

Table 27 quantifies the contribution of spatial/resampling corruptions to catastrophic failures. We define ‘‘Spatial/Resampling’’ augmentations as: upsample, downsample, elastic_transform, zoom_blur, rotate, shear, affine, perspective_transform, and pixelate (included as a resolution/resampling artifact that disrupts spatial structure).

Table 27. Fraction of catastrophic cases ($\Delta > 10$) attributable to spatial/resampling corruptions.

Dataset	Share from Spatial/Resampling (%)	Top Contributors
MMBench	65.5	upsample, elastic_transform, zoom_blur
MMMU-Pro	100.0	zoom_blur, elastic_transform, upsample

B.3. Mean Corruption Error by Category

Following ImageNet-C methodology, we compute mean Corruption Error (mCE) to compare model robustness against a reference baseline. For each corruption type c , $CE_c = \frac{\sum_s E_{c,s}^{\text{model}}}{\sum_s E_{c,s}^{\text{ref}}}$ where $E = 1 - \text{Acc}$ is the error rate. The reference model is the one with lowest baseline accuracy: **Gemma-3-12B** (85.3%) for MMBench and **Molmo2-8B** (31.2%) for MMMU-Pro. Values below 100% indicate better robustness than the reference; values above 100% indicate worse robustness.

Table 28 reveals category-specific robustness patterns. On MMBench, **Qwen3-VL-30B** achieves the lowest mCE across all categories (56–71%), demonstrating consistent robustness. Noise corruptions show the best relative robustness (mean 76.9% across models), while Binary transforms show the worst (mean 86.2%). Notably, InternVL3.5-4B approaches or exceeds 100% mCE in most categories (Blur 101.2%, Binary 100.8%), indicating it is less robust than the reference Gemma model despite having similar baseline accuracy.

On MMMU-Pro, all models cluster near 100% mCE (range 85–102%), reflecting the harder dataset where even the reference model struggles. **InternVL3.5-14B** leads with the lowest overall mCE (85.0%), showing particular strength in Color/Tone (83.8%) and Weather (83.9%) categories. Conversely, Gemma-3-12B exceeds 100% mCE in 9/10 categories (up to 102.3% on Blur), indicating worse robustness than the Molmo2-8B reference. The tight clustering suggests that on challenging reasoning tasks, relative robustness differences between models diminish.

C. Experiment Details

This section provides implementation details for reproducibility.

C.1. Random Seeds

We use fixed random seeds throughout all experiments to ensure reproducibility:

- **Sampling seed**: 42 — used for stratified dataset sampling to select the 20% evaluation subset.
- **Augmentation seed**: 1234 — base seed for deterministic per-sample augmentation. Each sample i receives seed $(1234 \times 1000003 + i) \bmod 2^{32}$ to ensure reproducible yet varied augmentations.

VLM-RobustBench: A Comprehensive Benchmark for Robustness of Vision-Language Models

Table 28. Mean Corruption Error (mCE, %) by model and corruption category. Lower is better; 100% matches the reference model. Reference models: Gemma-3-12B for MMBench, Molmo2-8B for MMMU-Pro. Categories match Table 1.

MMBench (Reference: Gemma-3-12B, Baseline 85.3%)												
Model	Base	Blur	Noise	Weath	Digi	Geom	Occl	Color	Resol	VLM	Bin	All
Qwen3-VL-4B	88.4	76.3	69.1	79.1	73.4	78.8	80.5	77.7	76.8	76.6	81.9	77.5
Qwen3-VL-8B	90.2	70.6	64.4	69.1	65.6	72.9	74.0	69.4	71.4	69.1	76.5	70.8
Qwen3-VL-30B	90.7	58.7	56.0	64.0	56.7	63.1	64.5	62.0	64.8	61.0	70.6	62.9
InternVL3.5-4B	86.3	101.2	93.6	99.0	96.0	98.8	99.2	96.7	99.7	94.9	100.8	98.3
InternVL3.5-8B	89.1	81.1	79.7	77.9	77.8	85.0	82.6	77.7	82.7	75.8	88.4	81.2
InternVL3.5-14B	86.6	93.2	86.0	91.1	89.3	91.1	94.2	91.7	92.2	86.4	98.2	92.0
Molmo2-4B	88.5	80.0	72.9	80.3	75.0	79.9	85.6	78.5	79.8	78.8	80.2	79.2
Molmo2-8B	88.4	79.5	70.1	76.9	77.4	80.5	81.0	77.8	81.9	75.1	79.6	78.2
Gemma-3-12B (ref)	85.3	100.0	100.0	100.0	100.0	100.0	100.0	100.0	100.0	100.0	100.0	100.0

MMMU-Pro (Reference: Molmo2-8B, Baseline 31.2%)												
Model	Base	Blur	Noise	Weath	Digi	Geom	Occl	Color	Resol	VLM	Bin	All
Qwen3-VL-4B	31.5	99.2	99.8	98.7	99.0	96.4	97.6	98.5	100.5	98.4	100.3	98.9
Qwen3-VL-8B	35.2	95.2	95.2	94.5	95.6	94.4	93.8	94.3	95.1	96.0	96.2	95.0
Qwen3-VL-30B	40.7	89.9	88.1	88.8	89.7	89.2	91.2	87.5	89.9	88.7	89.7	89.0
InternVL3.5-4B	37.3	94.8	92.9	91.7	92.5	92.4	94.7	91.6	93.9	93.7	94.6	93.2
InternVL3.5-8B	41.0	91.6	88.8	88.0	90.0	88.7	91.2	87.6	89.0	87.0	90.6	89.1
InternVL3.5-14B	42.0	86.6	84.8	83.9	85.5	84.2	85.8	83.8	86.0	84.4	86.5	85.0
Molmo2-4B	31.8	99.2	100.7	100.4	99.6	97.6	99.1	100.4	99.7	100.7	101.5	100.0
Molmo2-8B (ref)	31.2	100.0	100.0	100.0	100.0	100.0	100.0	100.0	100.0	100.0	100.0	100.0
Gemma-3-12B	33.0	102.3	101.8	101.1	100.2	99.5	101.9	100.1	101.6	101.0	101.9	101.1

- **Generation seed:** 42 — used for thinking-mode models that require sampling-based decoding.

C.2. Dataset Sampling

To reduce computational costs while maintaining statistical validity, we evaluate on a 20% stratified subset of each benchmark:

- **MMBench:** 869 samples from 4,329 total (stratified by `category` field)
- **MMMU-Pro:** 532 samples from 2,658 total (stratified by `subject` field)

Stratified sampling ensures proportional representation of all question categories/subjects in the evaluation subset.

C.3. Prompting Templates

We use two prompting modes with standardized templates:

Direct Mode. Designed for short, single-letter responses:

```
Please select the correct answer from the options above. Respond with only the
letter of the correct option. Do not explain. Answer:
```

Chain-of-Thought (CoT) Mode. Designed for reasoning-based responses:

```
Answer the preceding multiple choice question. The last line of your response
should be of the following format: 'Answer: $LETTER' (without quotes) where
LETTER is one of options. Think step by step before answering.
```

C.4. Generation Parameters

All models use deterministic decoding with `max_new_tokens=2048`. Thinking models (Qwen3-VL-Thinking) require sampling-based decoding and use: `max_new_tokens=8192, temperature=0.6, top_p=0.95, top_k=20`.

C.5. Augmentation Parameters

Table 29 lists the parameter values for each severity level across all severity-based augmentations. We evaluate at low, mid, and high severities. Binary augmentations have no severity variation.

Table 29. Augmentation parameters by severity level. Values at low, mid, and high severity are used in experiments.

Category	Augmentation	Param	Low	Mid	High	Note
Blur	gaussian_blur	radius	0.5	1.5	2.5	pixels
	motion_blur	ksize	5	9	15	kernel size
	defocus_blur	radius	1.0	3.0	5.0	pixels
	zoom_blur	factor	0.02	0.06	0.10	zoom amount
	glass_blur	sigma	0.5	0.9	1.3	blur sigma
Noise	gaussian_noise	std	0.02	0.06	0.10	normalized
	shot_noise	scale	25	10	5	lower=more
	speckle_noise	std	0.05	0.15	0.25	normalized
	salt_pepper	amount	0.01	0.04	0.08	pixel fraction
Weather	fog	intensity	0.2	0.6	1.0	opacity
	frost	intensity	0.2	0.6	1.0	opacity
	snow	intensity	0.1	0.3	0.5	density
	rain	intensity	0.1	0.3	0.5	density
	spatter	intensity	0.1	0.3	0.5	coverage
Digital	jpeg_compression	quality	80	50	20	lower=worse
	pixelate	scale	0.9	0.5	0.2	lower=coarser
Geometric	rotate	degrees	5	15	30	rotation
	shear	degrees	5	15	25	shear angle
	affine	degrees	5	15	30	rotation+scale
	perspective_transform	magnitude	0.05	0.15	0.25	distortion
	elastic_transform	alpha	30	80	180	deformation
Color/Tone	brightness	factor	0.7	0.3	0.1	lower=darker
	brightness_up	factor	1.3	1.7	2.5	higher=brighter
	contrast	factor	0.7	0.3	0.1	lower=flatter
	contrast_up	factor	1.3	1.8	3.0	higher=sharper
	saturation	factor	0.5	0.1	0.0	lower=grayer
	saturation_up	factor	1.5	2.5	4.0	higher=vivid
	gamma	factor	0.7	0.4	0.2	lower=brighter
	gamma_up	factor	1.3	2.0	3.0	higher=darker
	hue_shift	degrees	10	40	90	color rotation
color_jitter	range	0.1	0.3	0.5	random B/C/S	
Occlusion	random_occlusion	ratio	0.05	0.15	0.25	area blocked
	grid_mask	ratio	0.1	0.2	0.3	grid density
	center_occlusion	ratio	0.1	0.3	0.5	center blocked
Resolution	downsample	scale	0.75	0.35	0.15	lower=smaller
	upsample	scale	1.5	3.0	6.0	interpolation
	sharpen	factor	1.5	3.0	6.0	edge enhance
	posterize	bits	6	4	2	lower=fewer
	solarize	threshold	200	128	64	lower=more
VLM-specific	text_overlay	fontsize	24	48	72	pixels
	watermark	fontsize	24	48	72	pixels
	add_border	width	10	30	60	pixels

Binary Augmentations. The following 7 augmentations have no severity levels: flip_h, flip_v, grayscale, invert, channel_swap, equalize, autocontrast.

C.6. Augmentation Application

Augmentations are applied deterministically based on sample index:

1. For each sample index i , compute per-sample seed: $s_i = (1234 \times 1000003 + i) \bmod 2^{32}$
2. Initialize augmentation RNG with s_i
3. Apply augmentation to all images in the sample

This ensures: (1) identical augmentation across model runs for fair comparison, (2) different random variations per sample for stochastic augmentations (noise, blur, occlusion positions).

C.7. Evaluation Protocol

Correctness. A response is correct if the extracted letter matches the ground truth answer field.

Metrics. All metrics (accuracy, flip rates, RCE, mCE) are computed on the same 20% stratified subset across all models and augmentations, enabling direct comparison.

D. Augmentation Visualization

Figures 3–14 visualize all 49 augmentations applied to a representative MMBench image at low, mid, and high severity levels. Binary augmentations have no severity variation.

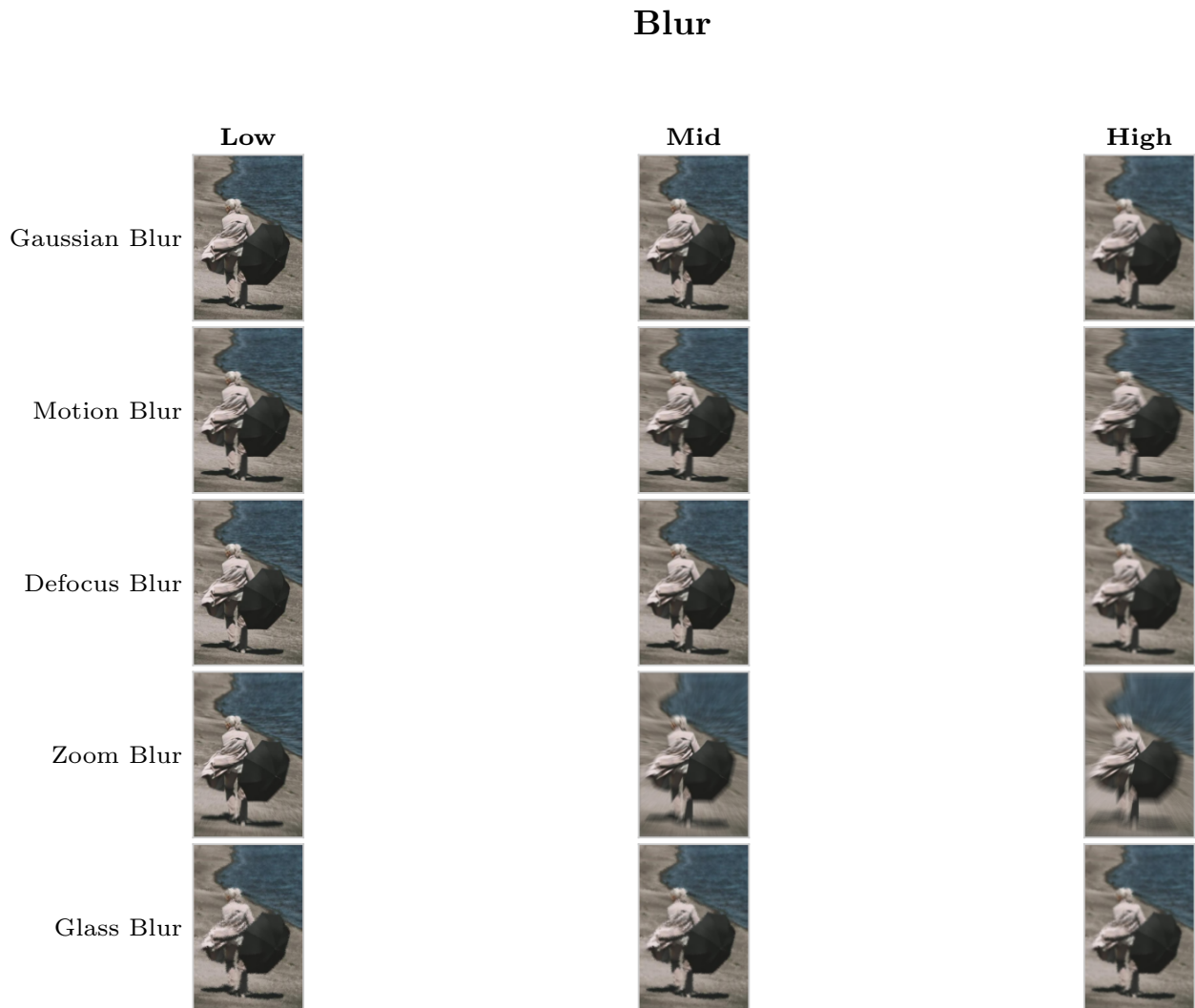


Figure 3. Augmentation Visualization: Blur augmentations at low, mid, and high severity.

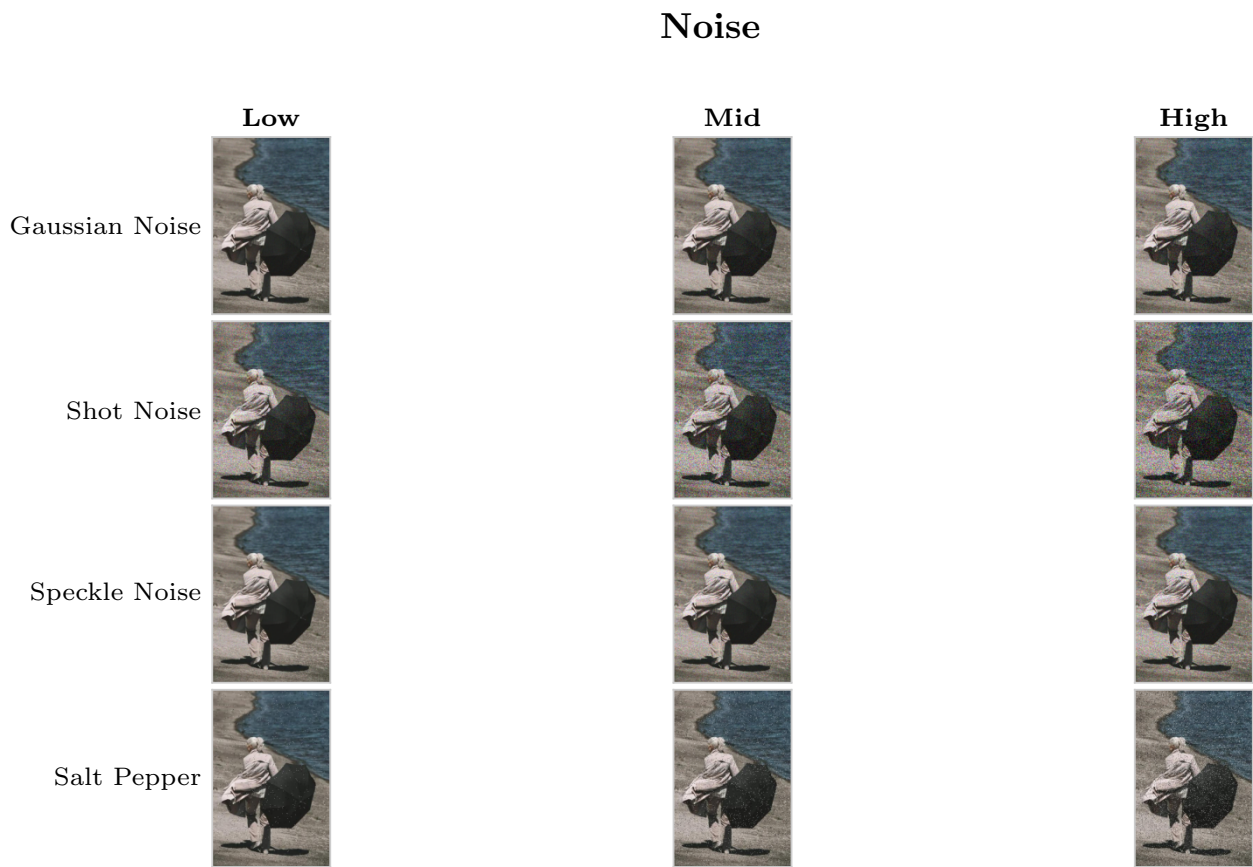


Figure 4. Augmentation Visualization: Noise augmentations at low, mid, and high severity.

Weather

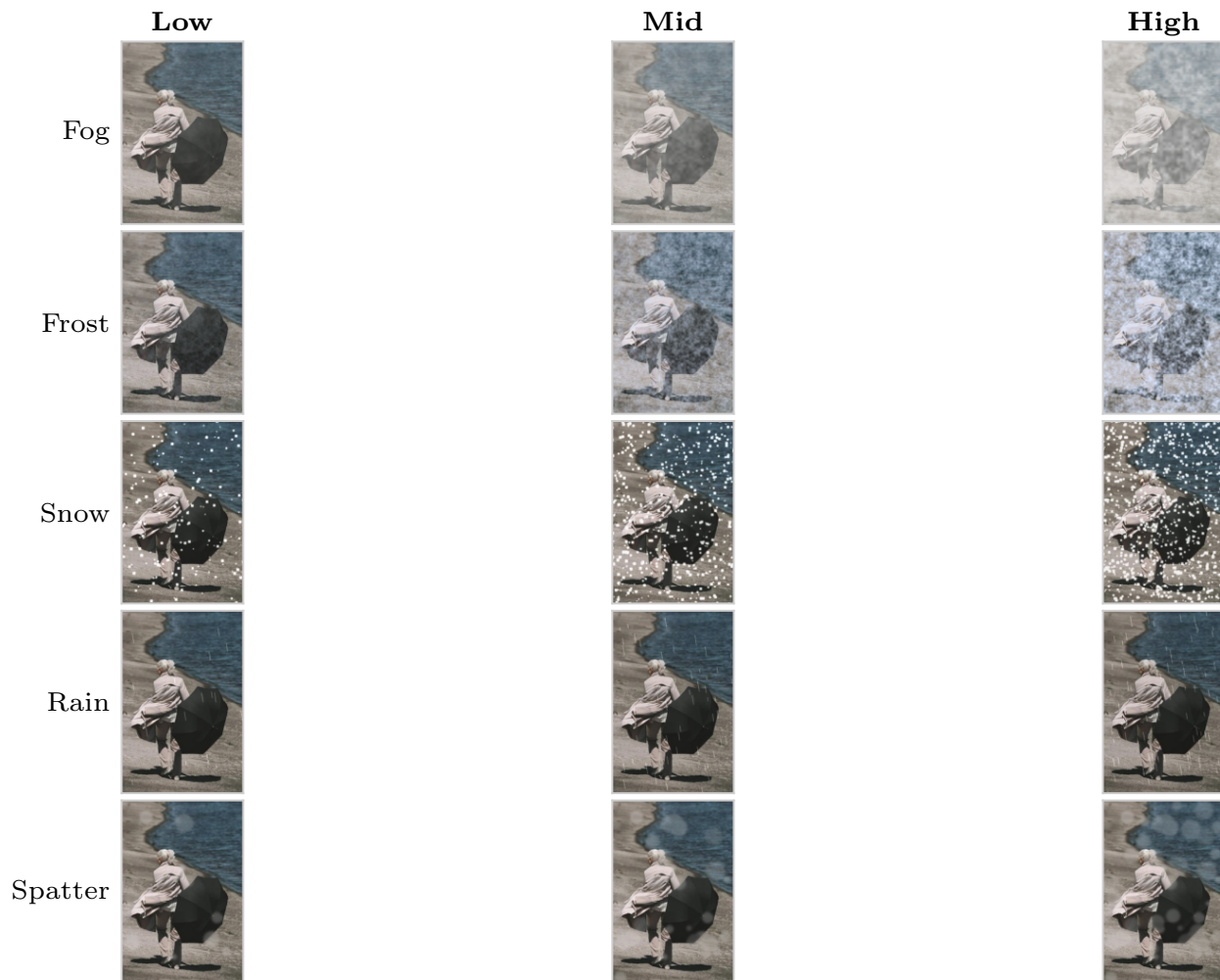


Figure 5. Augmentation Visualization: Weather augmentations at low, mid, and high severity.

Digital

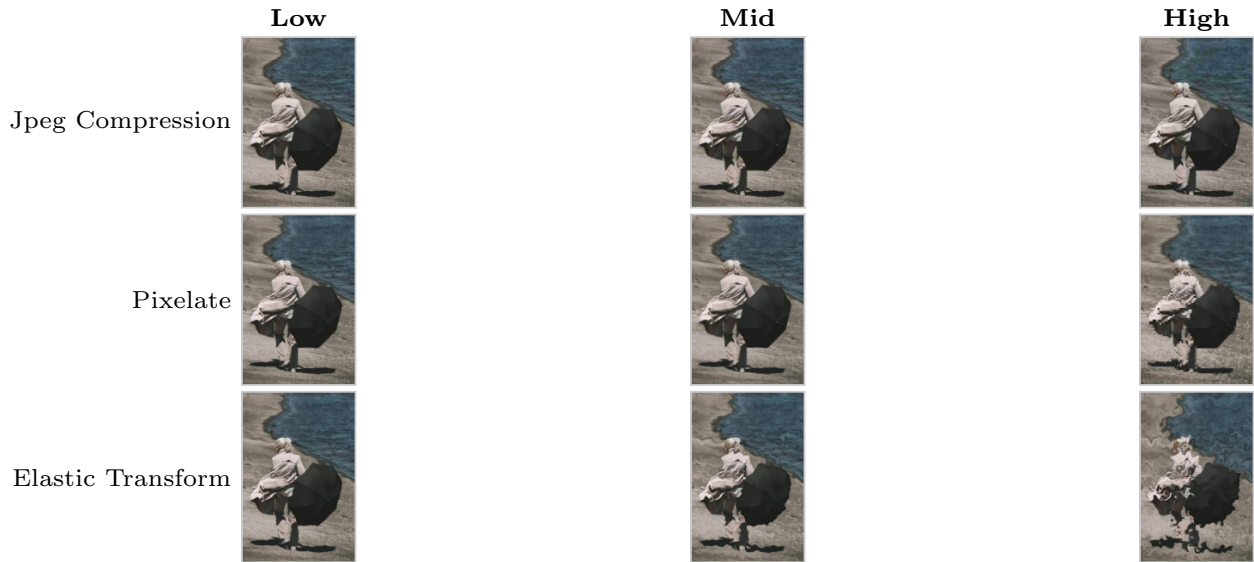


Figure 6. Augmentation Visualization: Digital augmentations at low, mid, and high severity.

Geometric

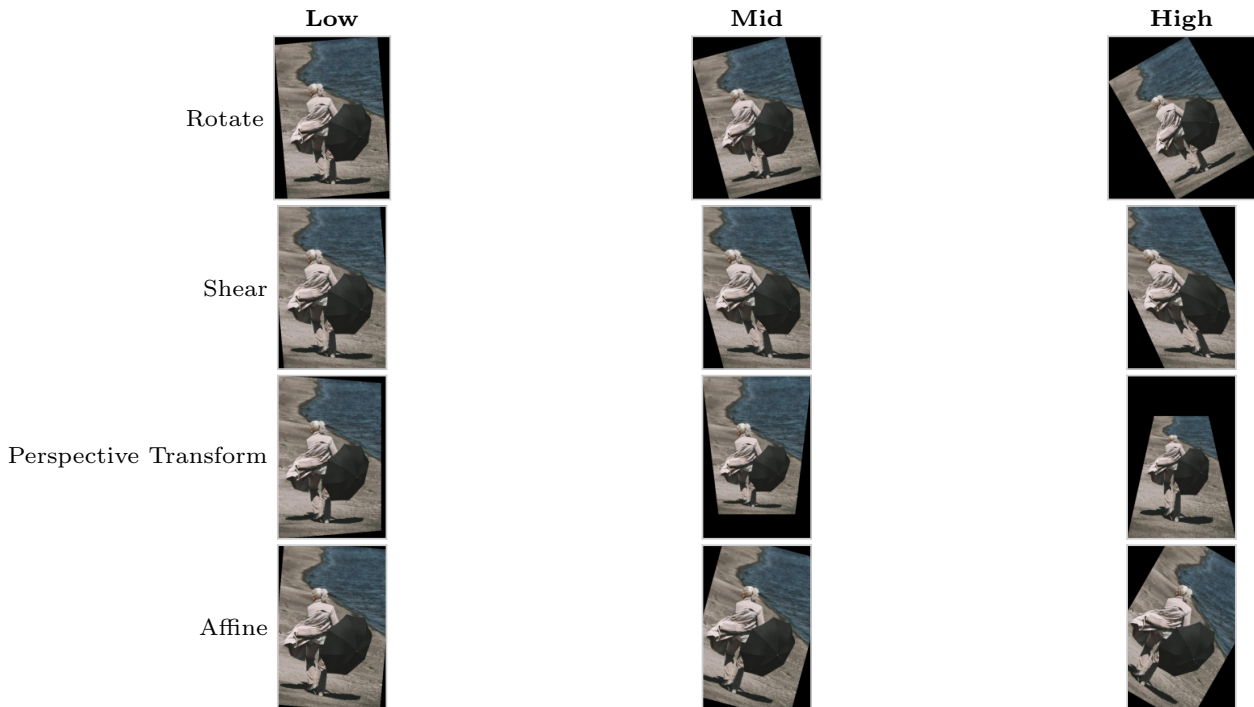


Figure 7. Augmentation Visualization: Geometric augmentations at low, mid, and high severity.

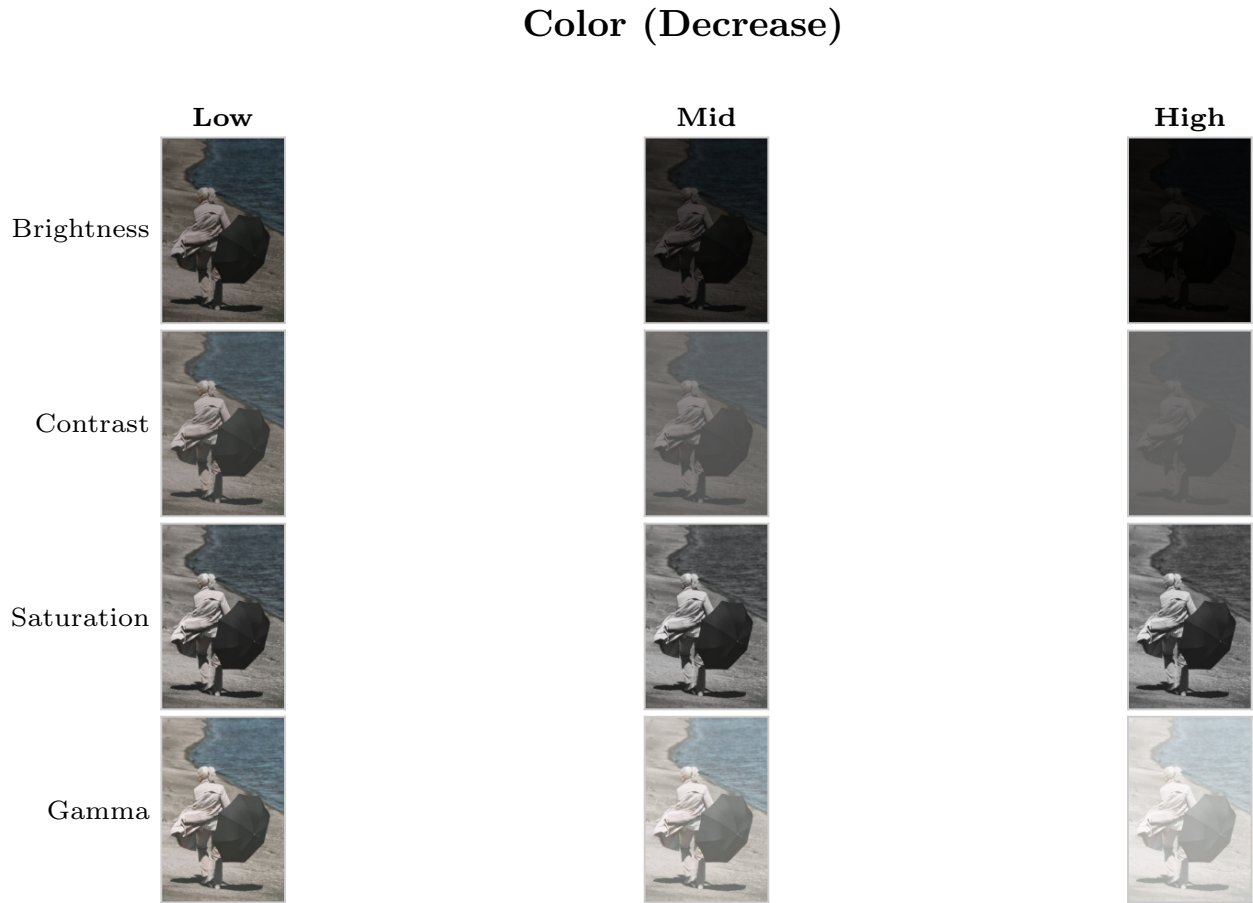


Figure 8. Augmentation Visualization: Color/Tone decrease augmentations at low, mid, and high severity.

Color (Increase)

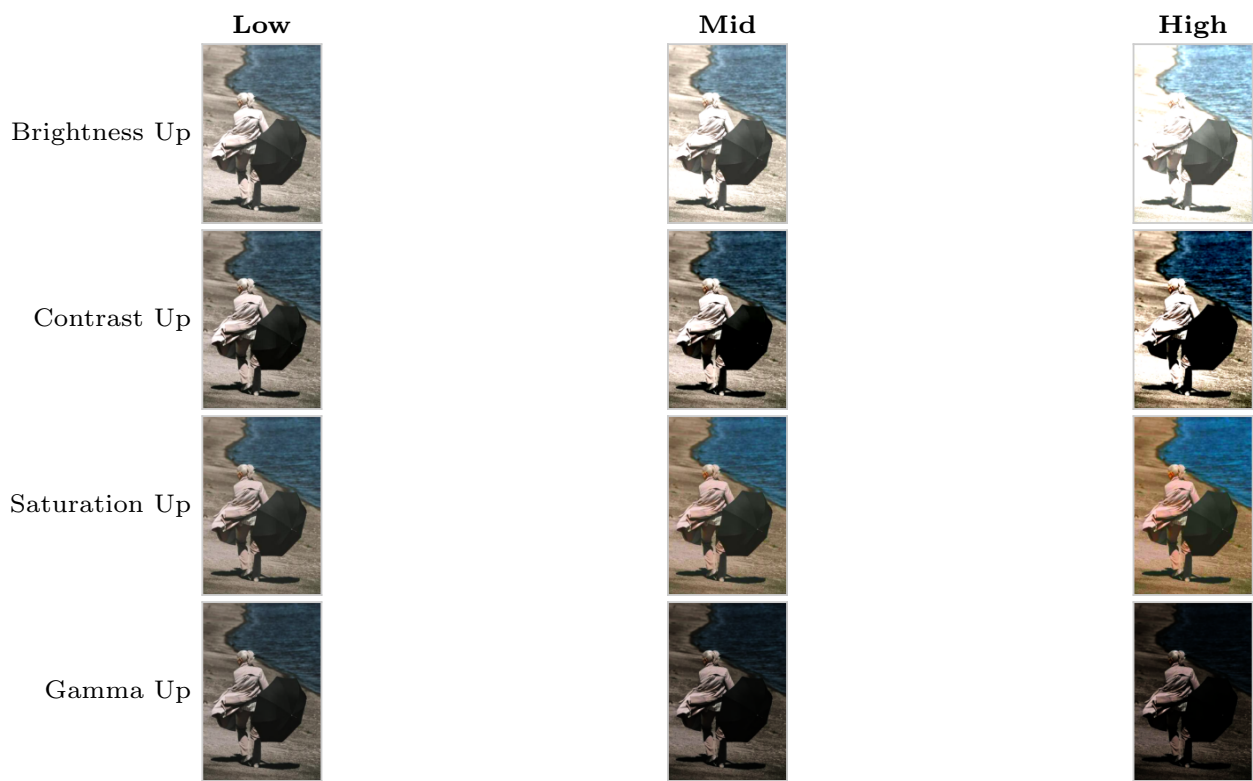


Figure 9. Augmentation Visualization: Color/Tone increase augmentations at low, mid, and high severity.

Color (Other)

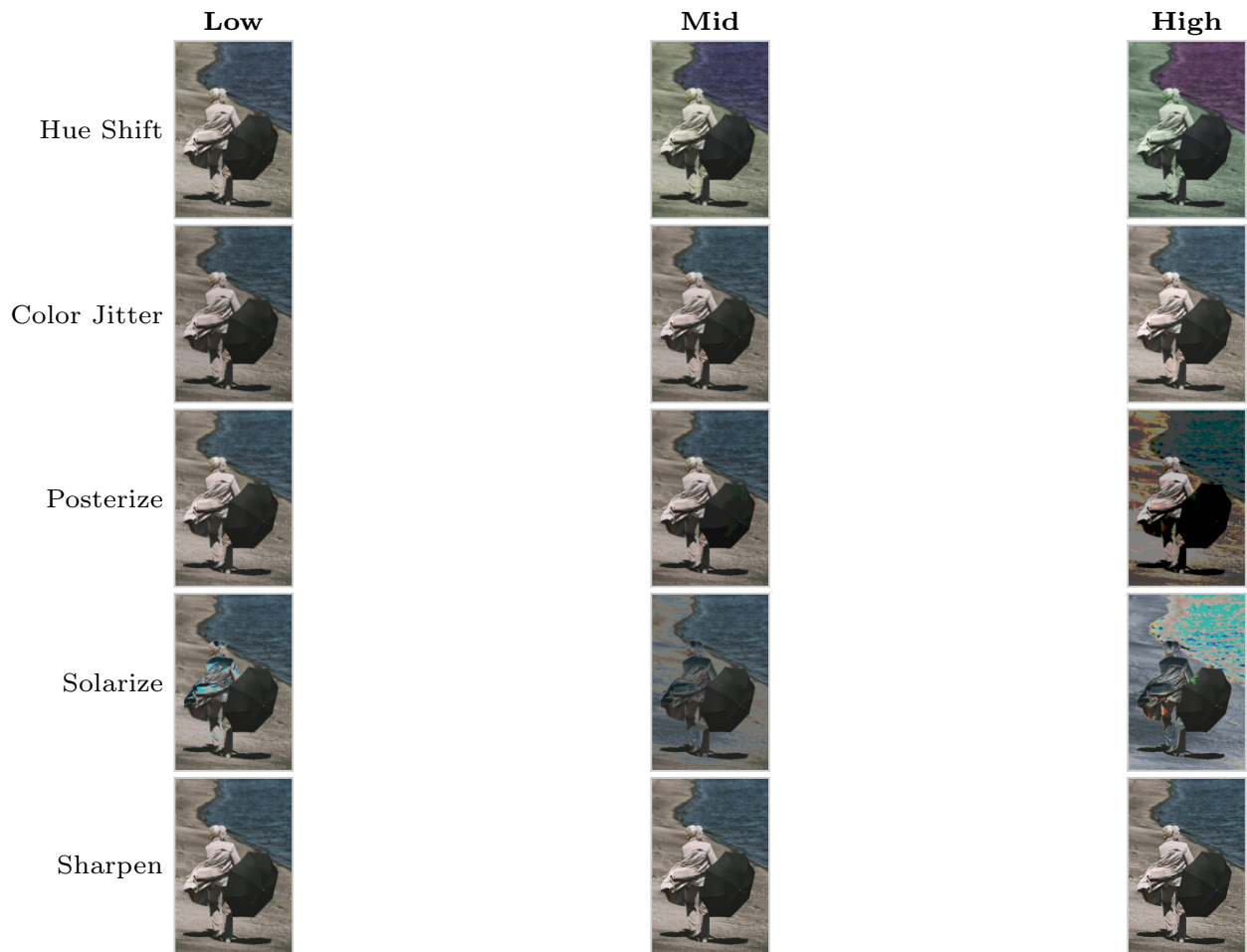


Figure 10. Augmentation Visualization: Other Color/Tone augmentations at low, mid, and high severity.

Occlusion

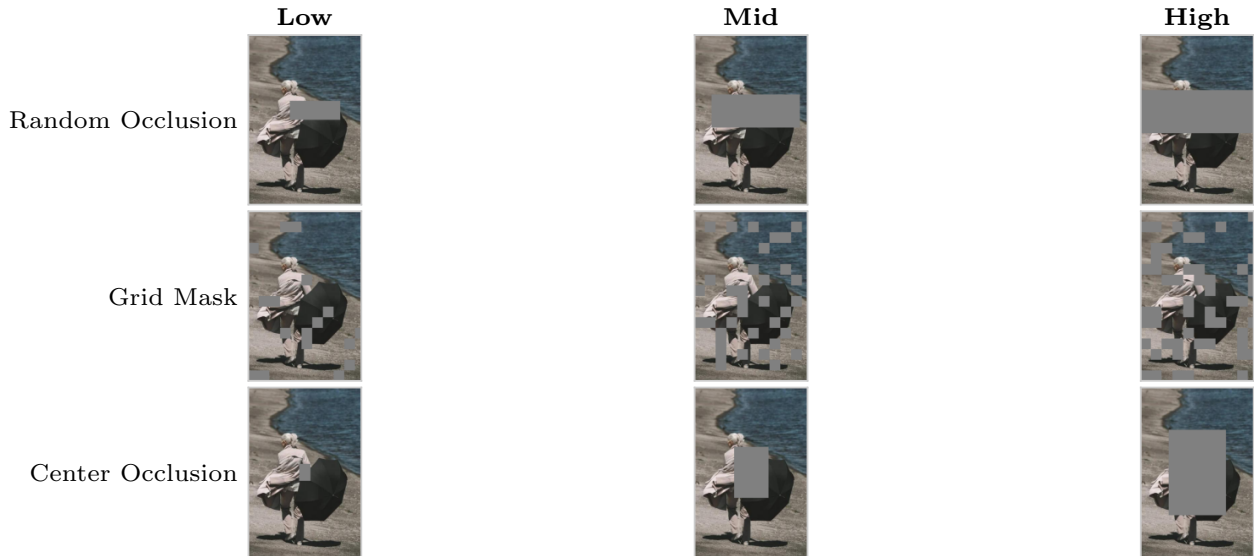


Figure 11. Augmentation Visualization: Occlusion augmentations at low, mid, and high severity.

Resolution



Figure 12. Augmentation Visualization: Resolution augmentations at low, mid, and high severity.

VLM-Specific



Figure 13. Augmentation Visualization: VLM-specific augmentations at low, mid, and high severity.

Binary Transforms

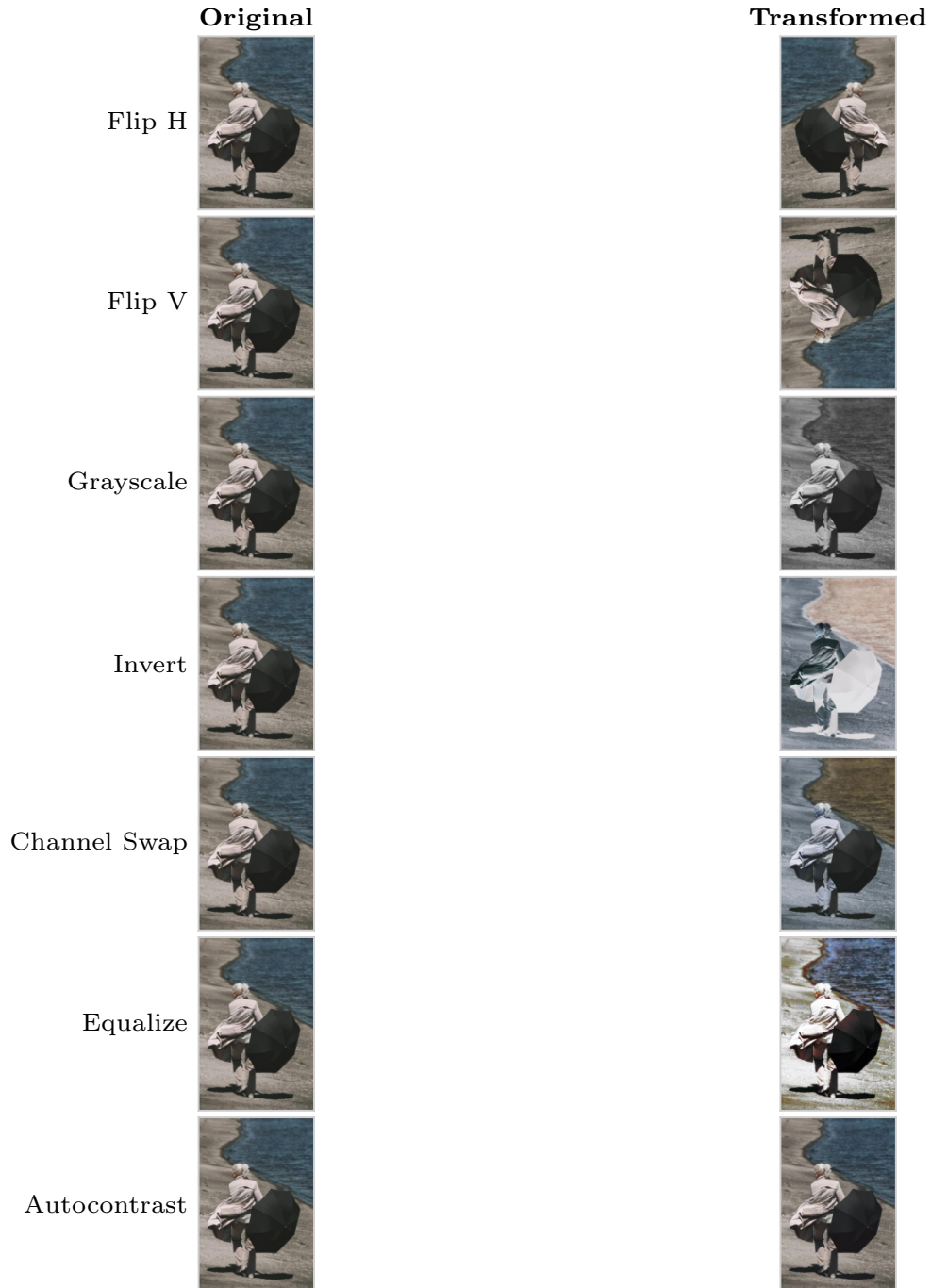


Figure 14. Augmentation Visualization: Binary transforms (no severity variation).